Universidade de Lisboa
Faculdade de Ciências
Departamento de Física

Development of a magnetic resonance compatible wrist device for the analysis of movement encoding in the brain

Mestrado Integrado em Engenharia Biomédica e Biofísica

Perfil em Engenharia Clínica e Instrumentação Médica

Diogo Duarte

Dissertação orientada por:
Doutor Jörn Diedrichsen e Doutor Hugo Ferreira

2016

Abstract

We interact with the world by moving our body: legs for locomotion, hands for dexterous tasks, and articulatory muscles to communicate. It is known that these movements result from patterns of electrical impulses in the nervous system. However, it is not yet known how the brain controls the fine aspects of movement. One important characteristic of movement control in the brain is directional tuning - a preferential neuronal response to an executed direction. In this work, we examine where and how the brain encodes movement directions in unimanual and bimanual movements in humans.

In order to address this question, we designed a motor experiment for directional movements. A hand device was developed in order to precisely monitor hand movements while 7 right-handed healthy participants executed a motor task. The task was built similarly to a game in which participants reached radial targets using wrist movements of one or both hands. After training, subjects executed the motor task in a magnetic resonance scanner.

Functional imaging data were acquired and analysed using novel multivoxel pattern analysis, in which we calculate pairwise dissimilarities of patterns of fMRI voxel activity across movement conditions. We tested for encoding of unimanual (contralateral and ipsilateral) and bimanual movements in cortical regions of interest. Kinematics data were also analysed to test for performance effects of direction and hand combination.

We found significant encoding of contralateral and bimanual movements in all tested regions. Ipsilateral movements were strongly represented in both hemispheres, except for right supplementary motor area and anterior-superior parietal lobule. Furthermore, the right (non-dominant) hemisphere encoded contralateral movements more preferentially than ipsilateral ones, when compared with the left hemisphere.

These results are in line with recent findings of well-defined ipsilateral movement representations. Future work will involve decomposing bimanual tuning functions in order to find a quantitative relationship between bimanual and unimanual encoding.

Resumo

A interação com o mundo é feita através de movimento - desde a locomoção até à comunicação verbal - tornando o controlo de movimento um dos aspetos fundamentais de maior interesse em neurociência. O controlo de movimento tem sido alvo de observação desde cedo em estudos comportamentais e neurofisiológicos, e sabemos hoje que os movimentos voluntários resultam de padrões de impulsos elétricos gerados no sistema nervoso. Contudo, não conhecemos ainda os aspetos mais precisos da geração de padrões de movimento nem a sua relação com parâmetros como direção, velocidade, etc.

Uma característica importante do controlo de movimento é a existência de *tuning* direcional - que consiste numa resposta neuronal preferencial a uma direção de movimento. Ao executar movimentos numa direção preferida, alguns neurónios despolarizam a uma frequência máxima, e a mesma diminui gradualmente à medida que o movimento se afasta da direção preferida. Este fenómeno foi caracterizado em 1982 em áreas motoras (córtex motor primário) ao serem executados movimentos direcionais do braço contralateral.

Contudo, estudos recentes mostram a existência de *tuning* direcional não só para o membro contralateral, mas também para o membro ipsilateral. Estas representações direcionais foram encontradas com medições electrofisiológicas ao nível celular, e também com técnicas modernas de imagiologia que medem sinal proveniente de volumes da ordem de mm^3, como ressonância magnética funcional. Com recurso a ambos os tipos de técnicas foram encontradas representações ipsilaterais bem estruturadas para movimentos ao nível do braço bem como dos dedos.

Desta forma, ambos os hemisférios cerebrais codificam movimentos direcionais de ambas as mãos. Sabemos também, por experiência quotidiana, que os movimentos bimanuais são bem coordenados, o que sugere que os mesmos são gerados tomando em conta informação de ambas as mãos. No entanto, a relação entre os padrões neuronais de movimentos bimanuais e unimanuais ainda não é clara.

Nesta dissertação pretende-se localizar e caracterizar *tuning* direcional durante movimentos unimanuais e bimanuais no cérebro humano. Desta forma temos como objectivo procurar quais as regiões corticais que codificam movimentos direcionais da mão contralateral, da mão ipsilateral, bem como as representações de movimentos bimanuais e a sua relação com movimentos unimanuais.

Para tal, foi desenhada uma experiência motora para testar movimentos direcionais, que foi executada em simultâneo com a aquisição de imagens de ressonância magnética funcional.

Foi desenvolvido um dispositivo para monitorizar de forma precisa movimentos da mão. De forma a assegurar compatibilidade com o ambiente em ressonância magnética, foram construídos dois manípulos ergonómicos com re-

curso a impressão 3D em *nylon*. Os manípulos foram equipados com sensores de rotação resistivos, e foram montados numa mesa de suporte desenvolvida para o efeito.

A fim de treinar os participantes e controlar a experiência, foi desenvolvido um protocolo motor organizado de forma semelhante a um jogo de alvos. Os participantes controlaram a posição de cursores num ecrã utilizando movimentos das mãos, monitorizados pelo dispositivo. O objectivo da protocolo motor foi atingir 6 alvos radiais com os cursores e voltar à posição central, com movimentos de cada uma das mãos, ou as duas (para todas as combinações de 6 alvos para cada mão). No total, a experiência consistiu em 48 condições de movimento - 6 movimentos radiais para a mão esquerda, 6 para a mão direita e 36 combinações bimanuais.

A experiência motora foi executada por 7 sujeitos destros saudáveis. Após uma sessão de treino, a experiência decorreu num scanner de ressonância magnética funcional Siemens Trio 3T, onde foram adquiridas imagens funcionais durante 10 repetições da experiência para cada sujeito. Adicionalmente, foram adquiridos dados de cinemática para as duas mãos durante as sessões de treino e de teste.

A análise de dados de cinemática consistiu na observação de tempos de reação e de movimento em cada condição. Comparámos condições unimanuais e bimanuais, testámos efeitos de direção, e ainda combinações bimanuais (movimentos simétricos, paralelos ou não relacionados). Para cada uma destas hipóteses foram usados os testes estatísticos aplicáveis. Não foram observados efeitos significativos nos tempos de reação, de forma consistente, para qualquer das condições em estudo. Pelo contrário, os tempos de movimento foram consistentemente sensíveis aos efeitos estudados.

As imagens por ressonância magnética funcional foram analisadas numa primeira fase conforme o procedimento tradicional. Este consiste no pré-processamento - envolvendo correções espaciais de efeitos de campo magnético, filtragem temporal, alinhamento com a imagem anatómica e segmentação. De seguida foi aplicado um modelo linear de forma de forma de independente para cada voxel (unidade discreta de volume) nas imagens. O modelo consistiu em 48 variáveis categóricas, correspondentes às condições de movimento em estudo, e 10 variáveis categóricas correspondentes às sessões de repetição da experiência. O objetivo deste modelo é a estimação dos pesos (β) da regressão linear, i.e., para cada condição é estimada a influência da mesma no sinal em cada voxel. De seguida é possível fazer inferência sobre os valores β - sob a hipótese nula de que são, em média, zero.

Procedendo desta forma, foi aplicado um teste t aos regressores β associados a movimentos da mão esquerda, direita, e movimentos bimanuais para as regiões: área sensorial somática I (S1), cortéx motor primário (M1), córtex pré-motor ventral e dorsal (PMv, PMd), área motora suplementar (AMS), lóbulo parietal superior, anterior e posterior (LPSa, LPSp) e córtex visual (V12). Foram encontrados valores de ativação predominantemente associados com movimentos contralaterais e bimanuais, e ativação menor em movimentos ipsilaterais. Os resultados coincidem fortemente com a perspetiva clássica de que cada hemisfério está associado a controlo da mão contralateral.

Contudo, os métodos univariados testam o quanto os voxels (ou regiões) variam a sua resposta com condições individuais, tornando a comparação entre condições de movimento difícil. Adicionalmente, estes métodos são indicados para o mapeamento de ativação perante estímulos, mas não para avaliar a estrutura da representação de condições, i.e., caracterizar respostas neuronais associadas conjunto de estímulos - como é o caso de *tuning* direcional.

Desta forma, foi aplicado um modelo de análise representacional no qual se pressupõe que os estímulos podem ser caracterizados por padrões de activação - neste caso correspondentes aos valores beta para cada voxel quando é executada uma condição. Neste modelo é calculada uma medida de (dis)similaridade entre todos os pares de condições. Neste projecto foi utilizada a distância Euclidiana, sendo que as comparações entre pares das 48 condições foram organizadas em matrizes de distância.

Os resultados revelam, qualitativamente, a presença duma estrutura de *tuning* direcional bem definida para movimentos contralaterais, bem como ipsilaterais. Também os movimentos bimanuais apresentaram uma estrutura de *tuning* bem definida e diferenciada entre regiões. De forma a quantificar e inferir acerca da presença de codificação direcional, os valores de distância correspondentes às condições contralaterais, ipsilaterais e bimanuais foram testados estatisticamente. Este teste assenta no pressuposto de que, perante a inexistência de codificação, as distâncias são zero (este pressuposto foi confirmado). Os resultados indicam uma forte codificação direcional de movimentos contralaterais para todas as regiões testadas. Este resultado é coincidente com estudos anteriores que encontram *tuning* direcional contralateral em todas as regiões em que o mesmo foi investigado. Contudo, encontrámos também uma forte codificação de movimentos ipislaterais, excepto na AMS e LPS anterior no hemisfério direito (não dominante). Estes resultados são coerentes com estudos recentes que mostram uma forte presença de codificação de movimentos ipsilaterais.

Os movimentos bimanuais estão também caracterizados por uma forte representação. Contudo, existe a hipótese de que estes estejam presentes apenas como consequência da codificação direcional de movimentos da mão contralateral (ou ipsilateral), e não directamente associados à codificação especializada de movimentos bimanuais. Esta hipótese é, contudo, de elevado interesse, já que uma codificação bimanual especializada pode explicar o mecanismo da coordenação bimanual. Desta forma, as matrizes de distância foram reorganizadas em termos de movimentos da mão esquerda e da mão direita. Os mapas resultantes foram comparados qualitativamente com simulações, revelando uma codificação bimanual maioritariamente associada com movimentos contralaterais. Contudo, a AMS e o córtex premotor ventral aparentam codificar movimentos bimanuais de forma não-linear, que poderá indicar alguma especialização em movimentos bimanuais que poderá ser útil para coordenação. Trabalho futuro envolverá avaliar quantitativamente estes mapas de forma a perceber quanta codificação bimanual é gerada de forma especializada.

Os resultados deste estudo coincidem com estudos recentes de codificação ipsilateral, e revisitam questões acerca da codificação bimanual. No futuro pretende-se decompor a codificação bimanual, avaliar de forma extensa e continua a superfície cortical, cerebelo e núcleos da base. Adicionalmente, esperamos executar futuras aquisições em novos participantes. Este tipo de estudo

pretende responder a questões no âmbito do controlo neural de movimento, que poderão ser úteis futuramente no contexto da reabilitação e controlo robótico. Consideramos também que os métodos de procura de codificação poderão ser utilizados para caracterização do sistema motor de sujeitos saudáveis em comparação com casos patológicos como acidente vascular cerebral, fornecendo um meio de avaliação dos mesmos.

Acknowledgements

I wrote this dissertation pointing me as the author, as academic rules dictate. However, developing and presenting research work is far from being a single-handed, lonesome task. This challenge involved many people to whom I'd like to express my most sincere gratitude.

I'd like to thank Dr. Jörn Diedrichsen for taking me in research group, for constantly challenging me and being a role model. With his help, I have gone further than I though I could. My gratitude also goes to Dr. Hugo Ferreira, for his help and advise, not only now but during my academic path. I would also like to thank Dr. Atsushi Yokoi, who welcomed me into this project. Besides teaching me many things, he became a friend and has been a wonderful work partner. I am also thankful to Dr. Naveed Ejaz for some of the most interesting discussions and company I've ever had. Many thanks to the remaining Motor Control Group members for welcoming me into the group, as well as the Institute of Cognitive Neuroscience IT staff, particularly Martin Donovan, not only for his technical help but also for his cheerfulness.

My family played a fundamental role in this project. My parents and sister accepted and supported me while I went abroad, even in the hardest of times. I will never be able to thank them enough, not only for the help they gave me, but for always believing in me and trusting my decisions.

I also wish to express my gratitude to my friends and fellow colleagues Ana Rita Moital and Carina Mendes, who made all these academic years much easier with their friendship and good mood. Thank you to my friends Ricardo Sousa, Nuno and Rafael Lopes for their constant support and cheerfulness over these years.

Finally, I'd like to thank Andreia Gaspar for all these years of happiness and fulfilment. She has always encouraged and believed me, through the best and worst times.

Contents

Chapter 1

Introduction

1.1 Context

The aspects of motor control result from electrical impulses generated by the brain - specific neuronal activity results in fine and precise movements. Several brain areas such as the motor cortex and the cerebellum are known to be involved in controlling motor functions both in planning and execution phases of movement [1].

However, we are not yet able to fully characterize movement encoding. Since 1982, we know some neurons are tuned to perform movements of the contralateral arm in certain directions, i.e., their firing (electrical impulse) frequency is maximal when an arm movement is performed in a preferred direction (PD) and gradually decreases when movements step away from the PD [2]. Even though the classical view is that each hemisphere controls the contralateral arm, several studies have shown that there is both arm and finger-specific activity in each hemisphere [3–5]. If each hemisphere contains information about movements of the both arms, how are bimanual movements encoded? Everyday experience tells us we can control both hands simultaneously with high accuracy in activities which require coordination such as tying shoelaces, driving, etc. This suggests bimanual movements are generated by taking into account information from both hands. In this case, bimanual movements might be encoded as a function of the analogous unimanual cases. Previous studies have addressed this question, but it is not yet fully clear how bimanual and unimanual movements are related [6, 7].

In order to further investigate how the brain controls movement, several research groups use robotic devices which allow precise measurements of movement parameters such as limb position, force and speed. Additionally, some of these devices allow imposing force fields or move limbs passively [7, 8]. Using such devices allows scientists to conduct motor experiments with well defined behavioural boundaries for movement direction, speed or reaction time, and they provide precise temporal data which can be analysed to assess kinematic characteristics of movement. Besides kinematics, it may be desired to mon-

itor neural activity. Several neurophysiology studies use direct measurement techniques such as single-unit recordings or electrocorticography (ECoG) [2–4]. This technique can be applied to non-human primates in an invasive manner and provides high temporal resolution at the cost of low spatial coverage, as a only limited number of electrodes can be placed in the brain.

Alternatively, imaging techniques such as positron emission tomography (PET) or functional magnetic resonance imaging (fMRI) allow broad coverage of brain volume at the cost of temporal and/or spatial resolution. In particular, fMRI can be used to localize activation areas during motor tasks and compare movement conditions [5]. This technique is characterized by high (up to whole-brain) spatial coverage, but low (on the order of seconds) temporal resolution and low functional signal-to-noise ratio. However, because it is non-invasive, fMRI is the predominant neuroscience technique for research in human subjects [9].

In this dissertation, we investigate how unimanual and bimanual wrist movements are encoded in the brain using a paradigm based on a classical motor task, monitored using modern devices and techniques.

This study allows us to characterize encoding of directions in the healthy human brain. Aside from the fundamentally neuroscientific purpose, it would be possible to apply it clinical context. Patients suffering from complications with motor impact, such as stroke, might benefit from close characterization of directional encoding during rehabilitation. Moreover, this knowledge could be used to improve the current state of brain-controlled devices which make use of directional features.

1.2 Objectives and Outline

In this dissertation we attempt to investigate the following questions:

- Which brain areas are directionally tuned for contralateral movements?
- Which areas encode ipsilateral tuning?
- Are there any areas specialized in bimanual tuning?

This dissertation describes the process conducted to address these questions. In Chapter 1 we present the context, relevance and outline of this dissertation.

Chapter 2 comprises three sections which introduce the relevant topics in this work: *a)* Section 2.1 outlines neuroanatomy and physiology concepts with focus on the motor system, and reviews neurophysiological, imaging and behavioural findings; *b)* Section 2.2 defines main concepts in functional MRI acquisition and data analysis. *c)* Section 2.3 briefly presents applications of robotics in motor control and overviews magnetic-resonance compatibility.

In Chapter 3, Sections 3.1 to 3.3 detail the process of building hardware and software for running the motor task. Sections 3.4 and 3.5 point out the most important aspects in the experimental paradigm, as well as the demographics of subjects included in the study. Behavioural and imaging data analysis methods are described in Sections 3.6 and 3.7.

Results are presented in Chapter 4, starting with behavioural/kinematics effects of bimanuality and direction in Section 4.1. Imaging results are presented in Section 4.2, spanning from traditional univariate maps to multivariate representation of movements.

Chapter 5 contains the discussion, which starts with some considerations about the experimental design, followed by interpretation of behavioural and imaging results. These are then compared to previous findings described in the literature.

The major conclusions in this study are presented in Chapter 6. Methodology is also discussed, and future work is suggested.

Chapter 2

Background

2.1 Neuroanatomy and physiology of motor control

The nervous system is responsible for movements, voluntary or not. Whereas non-voluntary movements can be generated by the spinal cord as a reflex, voluntary movements can be complex and their generation involves several brain regions [1]. Within the motor system, we can consider three major levels: spinal cord, brain stem and forebrain. In this dissertation we focus on forebrain level, particularly cortical areas such as the primary motor cortex (M1), somatosensory cortex (S1), supplementary motor area (SMA) and premotor cortex, which are located around the central sulcus. We also analyse posterior regions such as the superior parietal lobule and visual cortex.

This chapter introduces some of the concepts used in this work in order to analyse such a complex system.

2.1.1 Representation, Topography and Hierarchy

Representation

Movements, visual stimuli, speech and sensory stimuli are represented in the cortex. This means some neurons are active for certain sensations or actions - whether they are simple arm contraction movements or more abstract representations of visualized and executed tasks [1].

Each movement is then characterized by a pattern of neuronal activity which generates it [1]. Representations have also been shown not to be fixed in both animals with brain injury and in healthy humans [1, 10]. This is particularly important in post-stroke rehabilitation in humans, since representations can be changed even after short-term (1 hour) training [11].

Cortical representations are not, however, similar across subjects. Representations of finger movements, for instance, appear to be specific for each person,

that is, the pattern of activity for a specific movement is different across subjects [5].

The overall structure, however, is similar across subjects - the relative differences or similarities between movement patterns are identical [5, 12]. This means the way finger movements are organized in the cortex is similar across subjects, but the fine activation patterns for each finger vary. Furthermore, this representational structure seems to be driven by hand use [12].

Topography

The brain is functionally specialized - neurons are organized over the cortex according to their function. Neurons with similar functions, such as motor control, are clustered together in different sites than neurons associated with vision, for example [1].

Within each functional region, there is a topographical organization, i.e., there is a coherent organization within neighbouring neurons to encode a certain function. In the retina, for instance, there are retinal maps which encode a two-dimensional map of the visual field (retinotopy). Such organization is also present in the visual cortex. Likewise, sensory and motor maps also exist in several motor cortical structures, and can be represented by sensory and motor *homunculus* (somatotopy) [1].

The topographic organization is thought to be existing at birth, and optimized during development by reorganizing terminations in the corticospinal tract. This reorganization is likely to be modulated by use and sensorymotor consequences of movement [13].

In the scope of this project, the topographic organization of cells in the cerebral cortex is of particular importance. Neurons in M1 are clustered according with their preferred directions of movement, as demonstrated by Eiseberg [14] - this is what makes it possible for us to study directional tuning at voxel level in fMRI, where signal in each voxel is influenced by a large number of neurons.

Hierarchy

If movements are represented in several structures over the cortex, and this representation is well organized - how do the different cortical regions interact to control movements?

The classical view is that premotor areas generate complex multi-joint motor programs which are then sent to M1, where simple muscular control is achieved. In this case, movement parameters such as direction and velocity are represented in the neuronal population, both at muscle level or by coding an abstract workspace around the body [1, 15, 16].

However, there is also evidence that stimulating premotor areas generates grasping and exploratory-resembling movements, as tested with electrical stimulation in primates and humans [17,18]. This suggests that movement parameters

such as direction or velocity may be represented only indirectly - as argued in recent studies on the dynamical systems approach [19].

2.1.2 Directional tuning

Movement representations are specific to certain movement features. In the scope of this dissertation, we are mainly interested in the representation of directional tuning. In 1982 Georgopoulos et al. have shown, with single-cell recordings, that neurons in the motor cortex are tuned for directions. This means a neuron may have a preferred direction (PD) for which the firing frequency is maximal. When movements are performed in directions which step away from the PD, the firing frequency decreases gradually [2]. This concept is called directional tuning.

Directional tuning has been shown to exist in both 2D and 3D space, and the movement direction appears to result from coding of several neurons. The population vector is defined as the vectorial sum of preferred directions in 2D or 3D space, and the resulting direction from the population vector is highly similar to the real movement direction [20,21]. Directional tuning also exists not only for space, but also for isometric pulse forces and ramp-and-hold (gradually increasing) forces [22, 23].

There is a broad group of brain regions where directional tuning has been found, namely motor and premotor cortex, supplementary motor area, globus pallidus and cerebellum [24]. Directionally tuned regions have been found not only using single-cell recordings, but also with fMRI, in which each voxel contains a large number of neurons [4,25]. Finding directional tuning between such large neuron populations illustrates the topographic organization of the motor system.

Given that cells have preferred directions, several attempts of modelling their behaviour over direction have been made. Early models have cosine functions as a description of tuning functions [20]. However, alternative models with flexible tuning width and modality described tuning functions at cell level more accurately [26]. Tuning curves can also be modelled using Gaussian tuning functions [7, 27]. We should not, however, think of tuning functions as fixed representations - the tuning width of the whole population can vary with the experimental paradigm - more accuracy requires narrower tuning width [24].

Even though cells are tuned for specific directions, their referential is not always the same: cells have a certain preferred direction which refers to the muscular movements or an extrinsic axis of reference. The concepts of intrinsic and extrinsic coordinate frame were explored in the work of Kakei et al. [28]. In that study, primates performed wrist movements in different pronation/supination positions, so that moving in one direction would require different muscles depending on wrist position.This allowed the authors to distinguish between an intrinsic frame of reference, which refers to the body and muscular activity, and an extrinsic frame of reference (e.g., the room). There are intrinsic-tuned neurons which will fire mostly when a certain anatomical action is performed (e.g. extension of a certain muscular group) regardless of external coordinate

frames. Extrinsic-tuned neurons will respond maximally when a certain direction in an external frame of reference (e.g. to the left) is aimed, regardless of hand pronation/supination [28].

2.1.3 Bimanual coordination and ipsilateral activity

Everyday tasks such as cooking or tying shoelaces tell us both hands are move together in synchronized, but no necessarily similar manner. This phenomenon is known as bimanual coordination, and it's often associated with a related concept - bimanual interference. While bimanual coordination refers to temporal or spatial coupling in tasks such as swimming, interference refers to the difficulty in executing bimanual tasks such as the popular challenge of rubbing your stomach while tapping your head. Bimanual tasks can be very different relatively to the similarity between the movements of each hand: some are isomorphic tasks, such as pushing / pulling, and others are quite differentiated, such as playing the guitar. The diversity of tasks illustrates the flexibility in coordinating movements.

Behavioural insight

Behavioural studies show there is are bilateral movement constraints in space and/or time, phase in cyclic movements and homology [29]. There is a preference in the motor system for simple, integer combination rhythms of both hands such as 1:1 or 2:1. Even though it is possible to produce movements with polyrhythms, producing these movements requires training, and speeding the task pace causes these rhythmic patterns to fall back to simpler ones [30]. Bilateral patterns which deviate from phase or anti-phase synchronization also exhibit poor stability, indicating a preference for simple temporal relashionships, particularly 0°and 180° [29, 31, 32]. Movements with different amplitudes are also affected by bimanual coordination: when one of the hands performs movements with varying amplitude the other hand tens to move in a similar manner, despite being supposed to move with constant amplitude [29, 33]. Bimanual movements have also been shown to have a dependency on direction: if one hand moves vertically and the other horizontally, trajectories are clearly worse than when both hands move in similar directions [34]. Moreover, there is a directional preference when both hands move in mirror symmetric (intrinsic) directions and parallel directions (in extrinsic space) - timeseries of horizontal and vertical movement trajectories for all combinations were analysed with respect to phase coherence between both hands, and the results show better synchronization for mirror symmetric and parallel movements [35, 36]. There is a clear preference in bimanual control for intrinsic movements, which recruit homologous muscles [36]. However, extrinsic movements recruit different muscles, suggesting the motor system codes not only for muscles, but also for an external workspace (see Section 2.1.2).

Even though there are clear behavioural constraints for certain bimanual combinations, difficult tasks are possible to overcome through training [29]. Unstable phase modes in tasks similar to previously referred are possible to execute without falling back to in-phase modes when subjects are instructed to

maintain the pattern [37]. Furthermore, informing subjects with direct visual cues instead of symbolic text cues facilitates bimanual coordination [38]. This suggests bimanual control is highly dependent in the task engagement and in the cues given to test subjects. If bimanual control involves cueing and planning, what brain areas are involved?

Physiological and imaging studies

Part of the research in bimanual coordination focuses on lesions of certain brain areas in monkeys and humans. Lesion to SMA in monkeys caused duplication of movements in bimanual reaching tasks. In 1984, Brinkman proposed that this structure informs the contralateral hemisphere via the corpus callosum to prevent such duplication [39]. Tanji and colaborators also found neurons with different encoding of bimanual and unimanual movements in SMA and premotor areas [40], leading to the idea that SMA and premotor areas where the *loci* responsible for bimanual coordination.

However, in 1998, Donchin et al. tested target-reach movements in monkeys using a bimanual interface and found encoding of bimanual movements in M1. 69% of neurons probed in M1 showed bimanual specific activity and 64% in SMA, which suggested M1 is at least as important as SMA in bimanual control [3]. Cells in M1 were also more correlated to intended direction of movement than to muscle kinematics. These results challenged the idea that M1 is responsible only for low-level contralateral muscular control, and proved that despite important for bimanual coordination, SMA is not the sole responsible structure. Not only M1 and SMA are associated with bimanual movements: several researchers looked for differences between unimanual and bimanual movements by looking for activation and representation in both unimanual and bimanual conditions using fMRI, for executed and observed (visual input) movements. The results show that the networks responsible for unimanual movements are the same as for bimanual movements, confirming there are no bimanual-specialized structures in the cortex [41–43]. At the present time, the idea that bimanual coordination is controlled by specialized structures is not widely supported.

Instead, the prevailing idea is that several motor areas play a role in bimanual coordination and communicate via the corpus callosum [29]. In fact, callosotomy patients can move one hand vertically and the other horizontally with much more accuracy than a healthy control - i.e., without spatial interference effects [34]. Even though independence if facilitated in callosotomy patients, i.e., bimanual interference is reduced, spatial coordination of both hands is negatively affected - at least for novel tasks [34, 44, 45] . If both hemispheres communicate in order to couple bilateral movements, and if there is no specific *loci* that solely controls bimanual actions, what structures are involved in this network?

Koeneke and collaborators compared bimanual and unimanual movements in a coordination task: the bimanual case involved controlling a cursor with two homologous fingers, and the unimanual case required two fingers of the same hand. The results reveal no network specific for bimanual movements. In fact, the authors suggest that differences in the amount of activation are more likely to relate to task difficulty than to bimanual vs unimanual activa-

tion [41]. Alternatively, Debaere and collaborators investigated the activated areas in two bimanual motor tasks: one of the tasks included online movement feedback - this is the externally guided task. The internally generated task involved doing the same task, but with the eyes closed. For the externally guided task, superior parietal cortex (SPL), the premotor cortex (PM), the thalamus and cerebellar lobule VI were active, whereas basal ganglia (BG), the SMA, cingulate motor cortex, the inferior parietal, frontal operculum, and cerebellar lobule IV-V/dentate nucleus were active for the internally generated task. [46] In this study, two different bimanual conditions were studied with or without visual feedback. Because interference was reduced with visual feedback, it's not fully clear whether different activation patterns are related to internal and external representations, or to better spatial or temporal coupling caused by the existence of visual feedback [47]. The problem of spatial vs symbolic cues was revisited by Diedrichsen et al. in an fMRI study. The task consisted of performing unimanual and bimanual hand reaching movements in two directions: forwards and sideways. Bimanual movements could be either congruent (both hands forwards or sideways) or incongruent (one hand forwards and the other sideways). When evaluating the hypothesis *symbolic* > *spatial cues*, significant activation was found in posterior SPL, ventral premotor cortex and inferior frontal gyrus in the left hemisphere (strong lateralization). Furthermore, the comparison *incongruent* > *congruent* revealed significant activation in posterior lateral SPL and left inferior cerebellum [48]. It was suggested that SPL codes for spatial representation rather than for movement parameters - incongruent targets may require increased monitoring and more complex representation that targets which require homologous movements or parallel trajectories. The left hemisphere lateralization for congruency preference indicates lef themisphere specialization - in agreement with previous findings for complex tool use [47–49].

Ipsilateral representations

The classical concept is that each hemisphere controls the contralateral side of the body [1]. However, as discussed in the previous section, both hemispheres communicate via the corpus callosum for bimanual coordination. Consequently, during bimanual movements there are both contralateral and ipsilateral representations of movement [6].

However, the ipsilateral component has been shown to be present not only during bimanual movements, but also during unimanual ones [5, 50]. Ganguly and collaborators were even able to build a brain-machine interface by successfully predicting hand position from ipsilateral M1 activation [4]. In this case, what is the role of the ipsilateral representation during unimanual movemements?

One hypothesis is that this representation exists only due to passive outflow of information by inter-hemispheric communication [5]. Souteropoulos et al. stimulated the corticospinal tract and found no direct connection between this fiber bundle and the ipsilateral forelimb [51]. Moreover, Diedrichsen and Wiestler suggested that the ipsilateral representation is associated to mirror movements, and it needs to be suppressed in order to avoid them in bimanual actions [5].

An alternative hypothesis is that each hemisphere actively controls the ipsilateral arm [52]. Post-stroke recovery studies indicate that the ipsilateral hemisphere may play an important, yet maladaptative role in controlling the arm after stroke in the opposite hemisphere [53–55].

In this study, we will revisit both classical concepts and recent findings and compare them with our results.

2.2 Functional magnetic resonance imaging

The dominant technique in cognitive neuroscience is functional magnetic resonance imaging (fMRI) [56,57]. This functional neuroimaging method allows mapping brain activity correlates by comparing experimental conditions with rest. In fMRI, it is possible to cover a large brain volume divided across small volumes on the order of mm^3 - at the cost of poor temporal resolution and low functional signal-to-noise ratio when compared, for instance, with EEG [57]. Due to its non-invasive protocol and absence of time-consuming electrode placement, fMRI is more adequate to studies in humans where data acquisition in several brain regions in important.

In this section we will briefly overview the fundamental principles of nuclear magnetic resonance (NMR), BOLD contrast, fMRI designs and representational similarity analysis.

2.2.1 Principles of NMR and image formation

Hydrogen nuclei are used in magnetic resonance imaging for their abundance in the human body and adequate magnetic properties [56, 58]. In absence of a magnetic field, protons in the human body spin with random orientation. However, when placed in a magnetic field, hydrogen nuclei align with the field in one of two states: parallel or anti-parallel. This alignment takes the form of a movement called precession, in which the proton spin axis rotates around the magnetic field axis at the Larmor frequency [58].

The measured magnetization signal results from several protons - this is the net magnetization. Applying radiofrequency (rf) pulses causes protons to absorb energy, switching between parallel and anti-parallel states, and spin phase becomes coherent for all excited protons. After the rf pulse is applied, protons loose energy and phase coherence, and recover longitudinal magnetization [58].

The loss of transverse magnetization due to spin-spin interactions is characterized by the T_2 constant, intrinsic to the biological tissue. Because there are field inhomogeneities, the signal decays faster. T_2^* is the constant which comprises both effects. The recovery of longitudinal component is characterized by the T_1 constant, which is highly dependent of biological tissue, since it involves losing energy to the surrounding molecules (spin-lattice). T_1 is also dependent on the magnetic field, and T_1 values are usually much higher than T_2 values [57].

In order to select the anatomical volume to be imaged, spatial encoding is necessary. Gradients are applied to the magnetic field in order to modify

the Larmor frequency locally. Afterwards, *rf* pulses will excite protons within this slab. Space along x and y directions is encoded by magnetic and phase gradients [57, 58].

Pulse sequences are protocols for exciting and reading signal in MR. Knowing T_2 and T_1 constants of tissues allows to use different pulse sequences which emphasize T_1 or T_2 contrasts, by controlling parameters such as the *rf* pulse energy, repetition time (TR), etc.

The signal decay is detected by receiver coils, and has to be reconstructed to form an image. Because signals are acquired in k-space (frequency domain), images are obtained by converting to the space domain using the Fourier Transform [58].

Some sequences allow faster acquisition than others. In particular, the echo planar imaging (EPI) acquisition method uses repeated T_2^*-contrast sequences for fast volumetric coverage at the cost of high sensitivity to artifacts. Gradient-echo EPI is one of the methods used in fMRI due to fast acquisition of repeated volumes and the physiological properties it highlights [57, 59]. Neurophysiology principles and data processing in functional MRI are discussed in the next topic.

2.2.2 BOLD contrast and fMRI

Neurons in the brain take up oxygen perfused from the blood. Unlike oxyhaemoglobin, deoxyheamoglobin is paramagnetic, so it has a shorter T_2^*, which causes lower MR signal than oxyhaemoglobin because it distorts the magnetic field locally, increasing proton dephasing [57, 58]. However, higher metabolic activity areas have higher signal because the oxygenated blood supply to those areas overcomes their need in oxygen. As a consequence, MR signal is higher during activation than rest. This is known as the Blood Oxygen Level Dependent (BOLD) effect. However the observed change is, small, usually between 0.25% and 5% [9].

Because the signal-to-noise ratio in fMRI is low, carrying out an fMRI experiment involves several steps as introduced below.

Paradigm and fMRI designs

Due to low functional SNR, it is necessary to repeat the experimental conditions several times in fMRI to minimize noise across images. For each participant, several runs of the same experiment are conducted in two possible designs: blocked or event-related. Blocked designs involve executing conditions (motor tasks, visual stimuli, etc) for 10 to 30 seconds in an alternating pattern. Blocks are then convolved with the hemodynamic response function (HRF) and conditions are compared [56, 60]. Alternatively, conditions can be treated as events in event-related designs. In this case events are sorted randomly and separated by shorter time intervals than blocked designs. The hemodynamic response is then convolved with an event which is treated as an ocurrence in one timepoint (as opposed to a block or time interval) [60]. Blocked designs typically hold

better sensitivity, whereas event-related designs are allow more flexible *post hoc* characterization of events in regression models [56, 60].

Alternatively to behaviourally-clamped experiments, it is possible to continuously monitor free behaviour and include monitoring data as regressors in the fMRI model. This approach is not limited to the some of the constraints of conventional fMRI paradigms (in which natural behaviour is not present) and might be especially useful with uncooperative patients [57].

Preprocessing

Subjects move their heads within an acquisition, causing image-to-image voxel positions to vary. Head motion, even on the order of 1mm, can cause brain edge activation artifacts [56]. Furthermore, EPI data is sensitive to field inhomogeneities and affected by eddy currents which cause image distortion [58]. Moreover, the signal intensity over the brain volume is not homogeneous, as proton spins will be affected by the strength of the excitation field and proton density [56]. The previously stated effects have spatial consequences on data. However, there are also some considerations about how timeseries are affected: EPI acquisitions of a volume are carried in either interleaved or consecutive slice acquisitions. Because each slice is acquired at a different time, the HRF phase is captured differently in each slice. As a consequence, these effects should be corrected prior to timeseries modelling.

After image acquisition, the basic workflow for fMRI data preprocessing involves the following steps [56]:

- Slice timing correction
- Head motion correction
- Distortion correction
- Bias field correction
- Coregistration to anatomical image
- Temporal and spatial filtering

General Linear Model and Contrasts

The general linear model (GLM) expresses a dependent variable y as a linearly weighted sum of n explanatory variables x plus an error term ϵ [60]:

$$y = x_1\beta_1 + x_2\beta_2 + ... + x_n\beta_n + \epsilon \tag{2.1}$$

Or equivalently in matrix form for a set of y represented in matrix Y:

$$Y = X\beta + \epsilon \tag{2.2}$$

where X is the design matrix and ε is the variance-covariance matrix.

In order to obtain the regression coefficients, that is, estimating β, several regression methods which minimize the error ϵ can be used. Amongst them is the least-squares method, with matrix form solution [60]:

$$\hat{\beta} = (X^T X)^{-1} X^T Y \tag{2.3}$$

In fMRI, the GLM is commonly used in a massive univariate approach for each voxel, that is, each voxel is modelled independently. In this case, Y is the matrix of voxel signals at each timepoint after preprocessing and X is the design matrix [56,60]. The design matrix specifies regressors associated with the conditions of the experimental design: for each condition, a column can contain a label for categorical or quantitative characteristic in a condition. For example, a categorical label of animate or inanimate objects in a visual experiment, or a quantitative force level in a motor experiment could be included in the design matrix. These are examples of simple models - alternatively one could use HRF timepoints as regressors for each condition in the design matrix. It is possible to include not only the canonical HRF, but also its derivatives to account for subject-specific, session or region variations. Optionally, nuisance regressors such as head motion parameters or session-specific labels can be included. Read Friston et al. for detailed specification of design matrices [60]. After model specification, β must be estimated. In fMRI, the matrix of β values represents the contribution of the regressors for the measured signal at each voxel.

From the matrix of β values, statistical inference can be made. Contrast vectors, or matrices, allow us to establish hypothesis about our data by performing comparison operations between β values in different conditions [60]. In an fMRI study, such hypothesis could be whether a visual stimulus causes significantly higher activation than at baseline (no stimuli) or higher/lower activation than a stimulus B. After estimating the contrast, a statistical parametric map is obtained, representing t-values or F-values at each voxel - corresponding to the hypothesis that was tested. Packages such as SPM implement fMRI analysis from preprocessing to statistical inference [61].

2.2.3 Multivoxel pattern analysis

Traditional fMRI methods make inferences based on massive univariate models for each individual voxel. However, cognitive neuroscience methods have been focusing on multivariate models which treat the activity in several voxels as patterns for each condition [62] - an approach which has been named multivoxel pattern (MVP) classification, or multivoxel pattern analysis (MVPA) [63]. While traditional univariate methods focus on single voxel activation with the purpose of localizing brain functions, MVPA highlights how conditions are encoded in sets of voxels [62].

In MVPA, measures (or correlates) of voxel activity for each condition (or stimulus) are organized into vectors - if N voxels are included in the analysis, than each condition is represented by a vector of dimension N. These vectors are in a high-dimensional space, called representational space. In representational space, each value of activation can be, for example, the β value from the general linear model [63].

To conduct analysis in representational space, we can use classification methods and make inferences based of pattern discrimination - classification accuracy - for the classifier chosen [64]. Alternatively, we can calculate a measure of (dis)similarity between conditions - correlation or distances - which is called representational similarity analysis (RSA) [65, 66].

In RSA, a measure of dissimilarity between conditions is computed, resulting in a matrix of pairwise comparisons - a representational dissimilarity matrix (RDM). It is possible to make direct inference on each value (pairwise comparison) in the RDMs to test for significant difference between stimulus encoding; it is possible to compare RDMs between subjects or regions; and it is possible to test models of theoretical RDMs by regression. For more detail in RSA, read Nili et al. [66]. More details will be given in Section 3.7 on the application of RSA in this project.

2.3 Robotics in motor control research

Research in motor control often involves using robotic devices - they allow accurate measuring of motor parameters such as position, velocity and forces, and can also be used to impose force fields [67]. Some of these 2D arm-level robots are used to study the mechanisms of dynamic stiffness adaptation [68,69]. Similar robots can be used to investigate bimanual coordination (introduced in Section 2.1.3), both in primates and humans, and control of visual-motor interactions [3, 48, 70, 71].

In this work, a wrist monitoring device was built and a motor task software was implemented, resulting in a framework for wrist movement kinematic research.

2.3.1 MR-compatible devices

Combining robots and MR techniques can be useful for assessing clinical condition of patients through force feedback, haptic interfaces, mechanical vibrators for MR elastography or clinical surgery [72].

Some of the most challenging aspects of using robots in MR environment include the tight space for patients' body and robotic device inside the MR scanners and electromagnetic compatibility. Ferromagnetic materials should not be used in MR environment since they may become projectiles under the influence of the strong static magnetic field, or heat due to the influence of Eddy currents caused by switching magnetic field gradients (which can cause burns on the patient). Interference between both systems, leading to noise induction in external sensors and MR image distortions may happen. For this reason, materials used in MR environment inside the imaging area should have very low magnetic susceptibility. Nevertheless, small ferromagnetic components are acceptable if they are anchored and outside the imaging region [72].

Devices can be classified, relative to their possible use in MR environment, as MR-safe, MR-conditional or MR-unsafe devices. MR-safe devices pose no known risks when in MR environment, and MR conditional devices pose no known risks under specified conditions of use and MR-unsafe are known to pose risks [73]. In this dissertation, we describe the components which make the wrist device, justifying its classification as MR-conditional.

Several studies in cognitive neuroscience have used devices in MR environment and even fMRI studies in neonates for motor control [8, 73–75]. In adults, MR-compatible robots have also been used. Detailed information about one particular fMRI robot for arm movements can be found in [76]. This model was built using materials with low magnetic susceptibility for the structure and optical sensors which provide precise information about joint position. The framework for development of the wrist device in the present dissertation is similar to the arm robot - it shares the same input/output data acquisition unit and part of the same software code.

Chapter 3

Methods

In order to investigate directional movement representations in the human brain, human subjects were asked to make movements in several directions while functional MR data were acquired. The experimental task consisted of a game-like setup, where participants reach for several radial targets displayed on a screen. It contains three main components:

- Wrist device/manipulanda: used as a hardware interface for executing movements - the analogous of a joystick in a gaming setup.
- Task software: shows targets and cursor positions. Each cursor, left and right, is controlled by the corresponding manipulandum - analogous to a game.
- MRI scanner: Siemens Magnetom Trio 3T system was used for functional data acquisition.

The experimental setup is summarized in Figure 3.1.

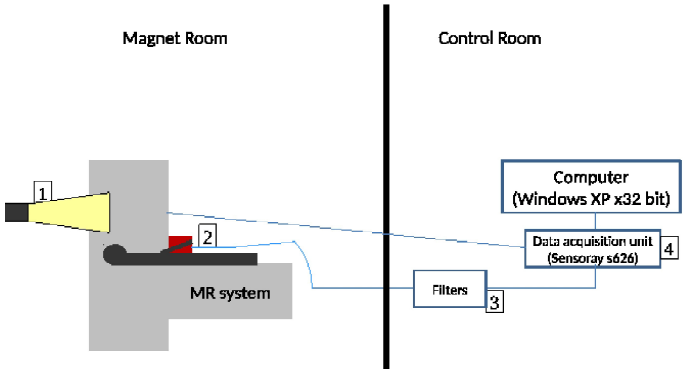

Figure 3.1: Diagram depicting the experimental setup. 1- Projector for visual feedback. 2- Wrist device, mounted over the participants' abdomen. 3- Filter box where the cables from the wrist device plug in. 4- Sensoray s626 data acquisition unit for analog sensor signal.

3.1 Wrist device

3.1.1 Wrist manipulanda

Because the task is performed in supine position for more than one hour, both in training and testing, the wrist device needs to be ergonomic. It was formerly designed by Esmaeili and collaborators, based on a fencing grip configuration [77]. The computer-aided design (CAD) files were kindly granted by the authors, and two handles - left and right - were 3D printed at the Bartlett School of Architecture, University College London. Both handles were printed using nylon selective laser synthering (SLS) for MR safety. Figure 3.2a shows the CAD for the wrist device, and the corresponding 3D printed version in Figure 3.2b.

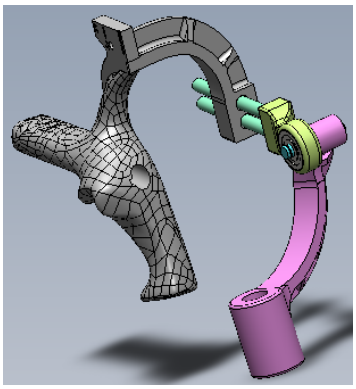

(a) Right hand ConfiGrip CAD design [77].

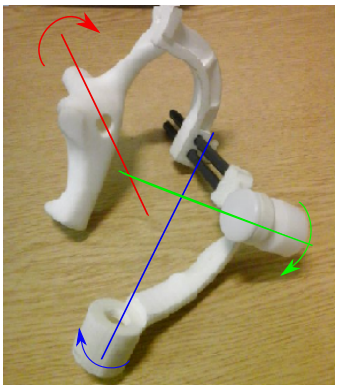

(b) Right hand wrist device handle SLS printed in nylon.

Figure 3.2: Wrist device handle. Pitch (green) and yaw (blue) movements are possible, but roll (red) is deliberately constrained by the device structure.

Considering the position of a resting hand grasping the device and pointing forwards, similarly to griping a fencing sword, there are two axis of rotation: horizontal (yaw) and vertical (pitch). Rotation (roll) is purposely restrained by the device design.

3.1.2 Support table

In order to mount the devices rigidly in the MR bed, a support table was designed in a CAD software (Trimble Sketchup) [78]. It serves two purposes: 1) mount the wrist devices onto it and support the weight of subject's hands; 2) tightly clamp wires and cables which connect the rotary sensors to the data acquisition channel. Figure 3.3 depicts the CAD design and the Delrin® plastic prototype.

The table is adjustable in height (12 to 18 cm), tilt (approximately $\pm$ 30°) and distance to/away from the head. This can be done by choosing between different slots on the Siemens Trio scanner bed, or for small adjustments, sliding

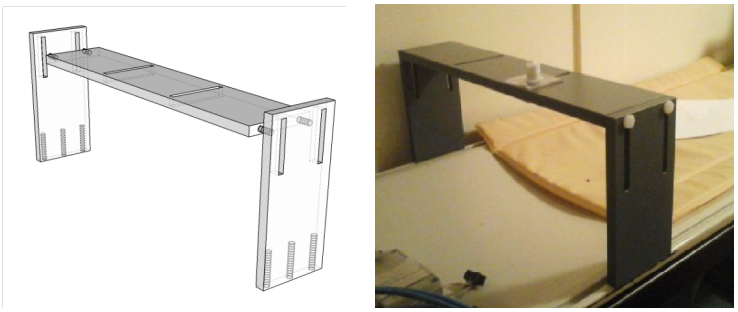

(a) (b)

Figure 3.3: **a)** CAD of the device table (software: Trimble SketchUp). **b)** Picture of the table used in the experimental setting (material: Delrin® plastic)

the acrylic base plates which hold the two manipulanda in place, on top of the table.

Both devices, manipulanda and table, were machined by Jonathon Henton at the Institute of Neurology, UCL. This process involved making parts such as the *manipulanda* length rods, base plates, mounting lids on the wrist manipulanda, and fabricating the support table. The base plates serve other purposes such as providing a stable mounting point for the horizontal axis encoder, and clamping cables which carry the encoder signal to the amplifier box.

3.2 Sensors, filters and data acquisition unit

Rotation sensors were used to precisely measure angular displacement. The Bourns 3382H potentiometer was the chosen model as it demands little space requirements - a consequence of it's dimensions (11 $\times$ 12 $\times$ 2 mm). The linearity tolerance is up to 2% signal and because it is a carbon-resistive 5kΩ potentiometer, amplification was not required [79].

Each encoder has 3 pins: ground (GND), positive voltage feed (V^+) and signal. GND and V^+ were connected to the output of a data acquisition Sensoray s626 card [80]. V^+ value was set to 5 volt, and signal value was read differentially with a ground pair between 0 and 5 V (16 bit resolution including sign).

Twisted pairs were used for electromagnetic interference reduction both in the flexible stranded wire and solid-core wire [81]. Two twisted pairs were connected to each of four (left and right $\times$ vertical and horizontal axis) encoders: GND+V^+ and GND+Signal. Stranded wire was used in the proximal sections of the manipulanda due to its flexibility, allowing free hand movements. Stranded wire is also mechanically compliant with constant bending and twisting, making it resistant to continuous use. It was then soldered onto solid-core wire in Shielded Foiled Twisted Pair (SFTP) cable. This cable is rigid as a consequence of solid-core wires - and therefore it was used for clampling onto the acrylic

plate for mechanical support. This is especially important for MR-safety, since no metal components should be left hanging free. (Figure 3.4).

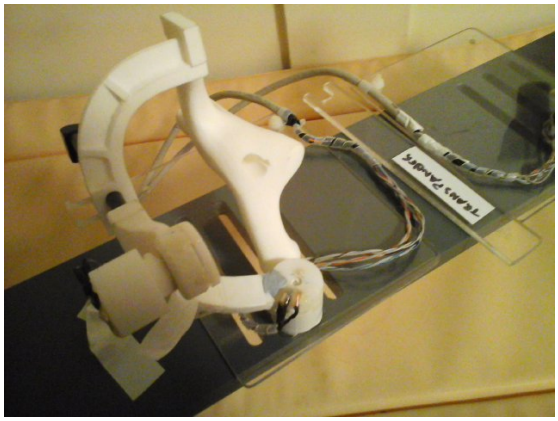

Figure 3.4: Left manipulandum mounted on top of the support table. For participants' protection, plastic lids and foam pillows covered wiring sections near the wrists.

Each cable, one for each device, has a female 10 pin circular connector used for legacy and compatibility with other devices in the laboratory. Long cables used in MR environment are then plugged into a DB25 connector in the breakout wall - between the magnet and in the control room - and are plugged into the filter box in Figure 3.5.

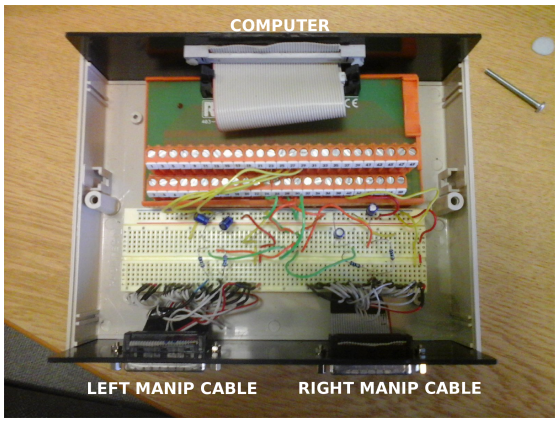

Figure 3.5: The filter box establishes connection between the two manipulanda and the computer, connecting to a DB25 rectangular connector as input from the manipulanda to a 50 pin connector as output towards the s626 card in the computer.

The filter box contains one low-pass 20 Hz cutoff frequency RC filter for each encoder, used for high frequency noise reduction in MR environment.

The filter box is then connected to the Sensoray s626 acquisition unit - V^+ is controlled, encoder signals are read, external counters are set and read, and

the repetition time (TR) counter is plugged in the computer for task-scanner synchronization.

3.3 Motor task

The motor task was programmed in a similar manner to a game - the user, in this case the test subject, has the objective of obtaining points. In order to get points, participants must correctly move one or two cursors towards radial targets accurately and within time bounds.

3.3.1 Structure

C++ was the programming language used to implement the motor task for legacy and compatibility with other tasks and devices already existing in the laboratory - similarly to some hardware components. Therefore, some of the C++ classes already existed in the laboratory and were integrated in the project structure.

Each experimental session contains several repetitions of individual motor tasks, referred to as **trials**. In this specific task they consist of individual reaching movements towards a radial target with one or two hands. Several directions have to be tested, so trials for all possible movement combinations are grouped into an experimental run - also called a **block**. During participants' training and testing sessions, several blocks with randomized trial entries are executed.

Over the course of the experiment, visual feedback is given to the experimenter and the participant through two separate screens. The participants' screen displays task-related objects and point feedback, as depicted in Figure 3.6.

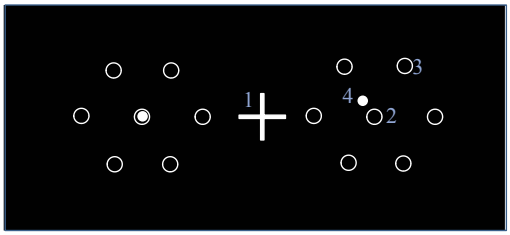

Figure 3.6: Visual elements in the participants' screen. 1 - Fixation cross; 2 - start box; 3 - target; 4 - cursor.

The experimenter screen displays the control shell with experiment variables:

- Subject name: name (reference) for each participant
- Block number: the run number for each participant
- Trial number: the trial number in each run
- Points: number of points in current trial and block
- TR: TR number for synchronization with the MR scanner

- State: the current state of the machine

3.3.2 State progression

To illustrate the task flow, the more relevant timesteps are represented in a flowchart (Figure 3.7).

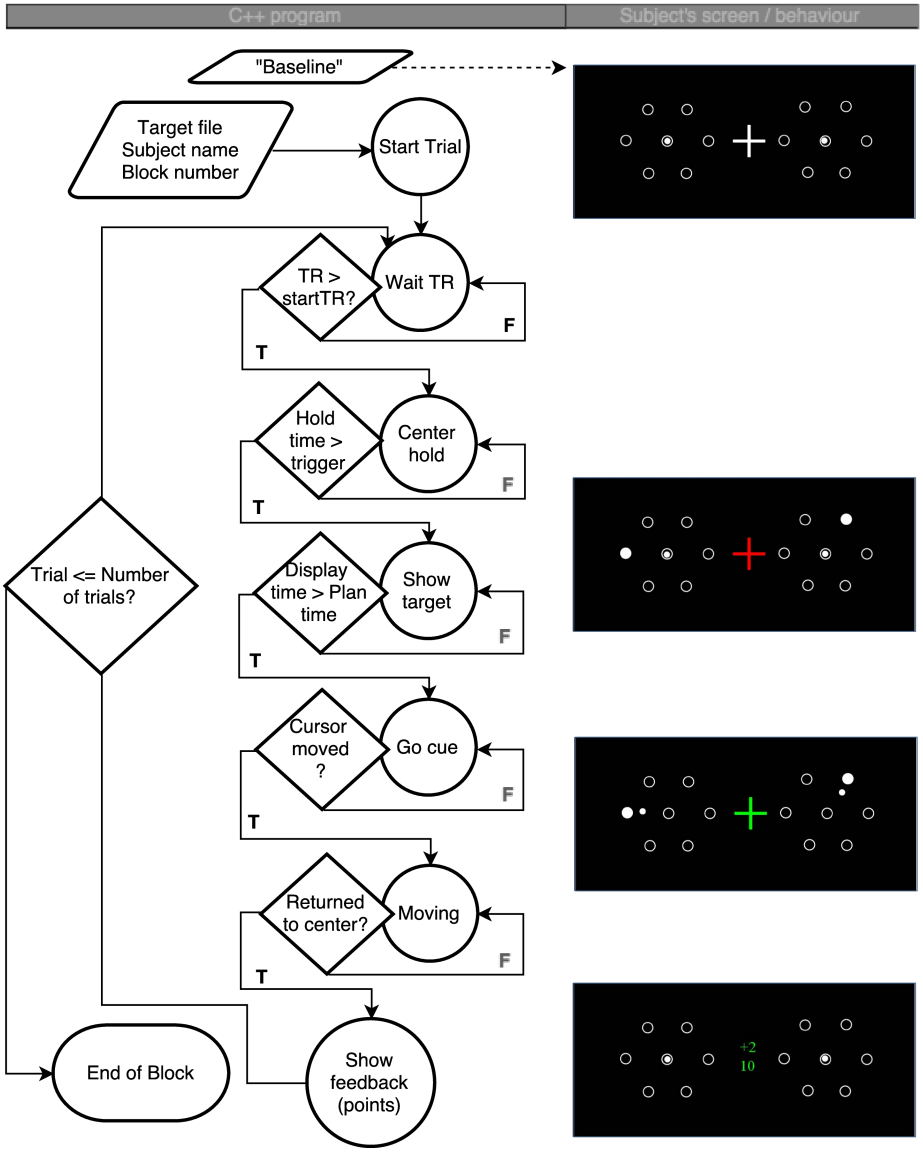

Figure 3.7: Flowchart indicating main states and decisions in the motor task software (left) and appearance of the participants' screen (right). Feedback is given by the fixation cross at the center of the screen.

Runs are executed as a group of trials, in which every trial is executed as

an iteration of the state machine in Figure 3.7. At the end of each block, a file with task information at every timepoint is created. Additionally, a file with summary trial-by-trial measurements for all blocks is created for each subject. Both these types of files were used for kinematics data analysis and general linear model specification in imaging data analysis.

At the end of each trial the participant's performance is evaluated as a **Good Movement** or not, and points are attributed accordingly. A Good Movement consists of a spatially accurate trial executed within all correct time bounds:

- wait in Start Boxes;
- move only after the Go Cue;
- start moving within maximum reaction time;
- execute the movement within limited time (reaching the target and returning to startBox).

One point is given per accurate target reach. In bimanual trials two points are required to make a Good Movement.

3.4 Subject information and Task Parameters

A total of 7 subjects participated in the experiment. Demographics and experiment parameters are presented in table Table 3.1.

Table 3.1: Participants' information and task-specific parameters used in the motor experiment.

Number of Participants	7
Gender	4 Females
Age (years)	27.7±5.1
Dominant hand	Right
Number of Targets	6
No. of Conditions	48
Trials per Block	96
Unimanual/Bimanual repetitions	2/2
Time per Trial (ms)	7
Time to plan movement	2000
Hold time in Training Mode (ms)	1500
Maximum movement time	1000
StartBox diameter / outer tolerance (cm)	1.6 / 0.5
Target diameter (cm)	1.6
Target radial inner/outer tolerance (cm)	1 / 0.5
Target radial tolerance from center (degrees)	10

3.5 Experimental protocol and data acquisition

Participants were recruited and accepted according to the following requirements:

- Age range : 18 to 35 years old
- Healthy
- Right handed
- 18 cm width from back to abdomen (able to fit in our experimental setup)

All participants were given an information sheet, specific to this project, containing relevant information about the study, objectives and protocol. After explaining the task to participants they were asked to sign the Informed Consent. A total of 3 sessions were conducted. The first session was for **training** - participants learned how to do the task by following instructions from the experimenter. Each participant used the setup as demonstrated in Figure 3.8, which shows the pronation position for the body and the resting position of the wrists. The latter blocks within the training session consisted mostly of performance optimization.

The remaining two sessions were carried out in MR environment, using Wellcome Trust UCL Siemens Trio 3 Tesla MR system. These correspond to **scanning** (or testing) sessions. The setup used in MR environment is similar to training. The device is adjusted in the MR room, and during Field-Map acquisition participants go through a practice run. However there is no communication between the experimenters and the participant within runs, except in the cases of technical failures or subject discomfort. Testing involves two sessions of 5 blocks each. Participants were allowed to rest between runs according to their own will. All subjects were reimbursed for their time during the experiment plus a bonus proportional to the points achieved in the motor task.

3.6 Kinematic analysis

Behavioural data analysis consisted of analysing timeseries of kinematics for different conditions. Analysis was conducted in Matlab® 2012b language/environment using files from the C++ program output. Kinematic measures of position for both *manipulanda* were recorded at every 5 ms, corresponding to a frequency of 200 Hz.

We are mainly interested in comparing directions/conditions of movement with respect to movement time (MT) and reaction time (RT). Particularly, we can ask specific questions which relate to Section 2.1 such as:

- Are unimanual and bimanual movements different?
- Does direction of movement affect performance?
- Are intrinsically related bimanual movements performed better than extrinsic or unrelated?

These questions were addressed by comparing: *a)* Unimanual vs Bimanual conditions; *b)* Directions of movement; and *c)* Mirror-symmetric, Parallel and

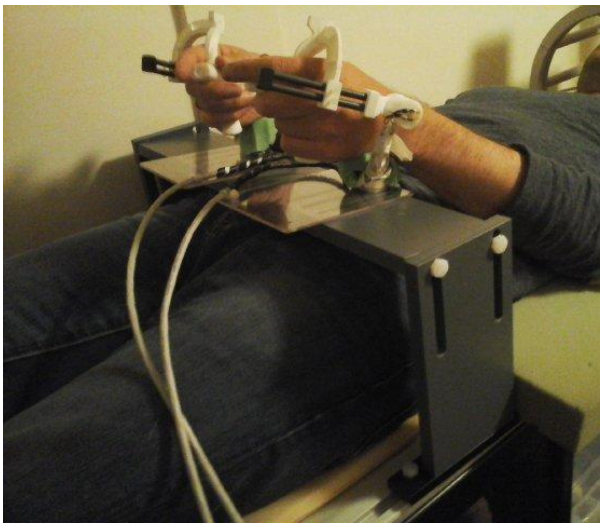

Figure 3.8: Device in use: resting position adopted by the participants. This particular example corresponds to the training setting. Anatomical variability is covered by hardware adaptations discussed in Section 3.1.

directionally unrelated movements. These conditions were evaluated with respect to kinematic performance variables recording during training and testing conditions - reaction times, movement times and hand decoupling.

Reaction time was obtained by a state transition: from *center hold* to *moving* states. In the motor task, this is triggered by any of the cursors exiting the *start box*. Movement time is calculated from the duration in state *moving* - in the motor task it corresponds to the time interval between leaving the *start-boxes* and returning to them after hitting the target. Additionally, decoupling was calculated by adding the time difference at movement start and end during bimanual movememts. Decoupling was applied to bimanual combinations (intrinsic, extrinsic and unrelated) only.

Results are presented in section 4.1 visually, and applicable statistical test results are shown for each case.

3.7 fMRI data analysis

fMRI analysis was conducted in Matlab environment using SPM8© package and the RSA Toolbox [82]. Additional Matlab routines were written in the Motor Control Group with Atsushi Yokoi and Jörn Diedrichsen.

3.7.1 Preprocessing and GLM

Preprocessing was conducted according with the following order:

- Slice timing correction

- EPI realignment and unwarp (distortion correction)
- Field bias correction
- Functional to anatomical image registration
- Anatomical image segmentation (white and grey matter)

Coregistrations to anatomical images were based on manual definitions of EPI image position. Upon GLM specification, functional data was high-pass filtered in the time domain at 128Hz, without spatial filtering.

The general linear model was specified with 48 categorical variables of interest - corresponding to 48 conditions in our event-related experiment. The onset for each stimulus was imported from motor task files, as well as the condition label for trials. The design matrix X (equation 2.2) contained one regressor per trial per timepoint - resulting from HRF convolution with boxcar function - and one additional regressor per session:

$$\underset{(T\times P)}{\mathrm{Y}} = \underset{(T\times K)}{\mathrm{X}} \underset{(K\times P)}{\beta} + \underset{(T\times P)}{\epsilon} \tag{3.1}$$

Where T is the number of timepoints (or scanner TR's), P is number of voxels, and K = number of conditions $\times$ number of sessions + nuisance regressors (in this case, one per session).

Estimation of β values (regression coefficients) was performed using the SPM package, which implements the Restricted Maximum Likelihood algorithm [83]. After estimation, $t-$contrasts against rest were calculated for each condition, and also for Unimanual Left, Unimanual Right and Bimanual movements.

These contrasts were mapped for each subject on a cortical surface which was reconstructed using FreeSurfer software suite [84]. Surface maps with overlayed contrasts were visualized using Caret software [85].

3.7.2 Representational dissimilarity analysis

Experimental conditions were compared using RSA after GLM estimation. We will now introduce the rationale for using RSA in this project.

Each condition - hand movements in this case - is characterized by a pattern of neuronal activity [65]. Since cortical functions are organized in a topographical way, we would expect groups of neurons which encode similar conditions to be anatomically close [1]. In fact, it is possible to detect directional tuning at voxel level using fMRI, which relies on activity in discrete volumes on the order of mm^3 scale volume [4].

If a cortical region encodes a certain stimulus (visual, motor, etc) this region will therefore exhibit distinct activity patterns for the conditions it encodes. For each condition, there is an activity pattern U_i which can be represent as a vector with an activity value for each neuron or voxel. A set of conditions can be concatenated into a matrix $U_{(N\times P)}$ where N is the number of conditions and P is the number of voxels.

One way of assessing the dissimilarity between conditions is to compute the Euclidean distance in voxel space [65]. One can calculate the inner product matrix of U:

$$G = UU^T \tag{3.2}$$

where each element $G_{i,j}$ is the inner product between conditions i and j. The G matrix sustains information about the distance of each pattern to baseline activity in the diagonal. Additionally, it is possible to calculate the squared Euclidean distance from G in each point [86]:

$$D_{ii} = G_{ii} + G_{jj} - 2G_{ij} \tag{3.3}$$

where D is the distance matrix calculated from the patterns U. By definition, all values in the diagonal of D are zero and the matrix is symmetric. The upper or lower triangular of D contains the pairwise distance between all conditions in U.

From this point onwards we will refer to distance matrices and representational dissimilarity matrices (RDMs) indistinctly. However, RDMs can be calculated from any measure of dissimilary between two patterns, such as 1-minus-correlation, angle distance in voxel space, etc [66, 87].

RDM Simulations

Given a directionally tuned set of voxels, what is the structure of a theoretical RDM? This question was addressed by simulating the voxel response for equally separated directions. Given a set of voxels, we assign to each one a preferred direction φ. The tested directions are θ, which would be the directions for movements executed in an experiment. The simplest voxel response would be when the voxel only exhibits activity $a_{\theta,\varphi}$ if the tested direction matches its preferred direction:

$$a_{\theta,\varphi} = \begin{cases} 1, & \text{if} \quad \theta = \varphi \\ 0, & \text{otherwise} \end{cases} \tag{3.4}$$

In this case, U is given as a matrix of $a_{\theta,\varphi}$:

$$U = \begin{bmatrix} a_{\theta 1,1} & \cdots & a_{\theta 1,P} \\ a_{\theta 2,1} & \cdots & a_{\theta 2,P} \\ \vdots & \ddots & \vdots \\ a_{\theta N,1} & \cdots & a_{\theta N,P} \end{bmatrix} \tag{3.5}$$

where N is the number of conditions (or θ directions) and P is the number of voxels. In U, rows are **activity patterns**, and columns are voxel **tuning functions**.

The symmetric distance matrix calculated using equations 3.2 and 3.3 will have, by definition, diagonal equal to zero. The off-diagonal values will yield

some value which will depend on how distant the patterns are in voxel space. In this case, all patterns are equally distinct (Figure 3.9). This is equivalent to having a tuning function as narrow as possible, i.e., a Dirac δ.

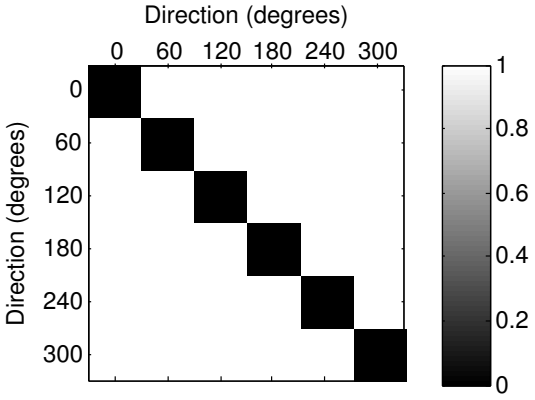

Figure 3.9: RDM for simulated patterns with narrow tuning function. Tested movements (θ) spanning from 0° to 300°.

If we assume our set of voxels is in the left cerebral hemisphere and codes both contralateral and ipsilateral movements, we can represent the RDMs for contralateral and ipsilateral movements together (Figure 3.10). In this RDM, conditions 1 to 6 refer to left hand movements, and 7 to 12 refer to right hand movements in similar directions (Table 3.2). The first and third quadrant represent unimanual left and right movements - similarly to Figure 3.9. The second and fourth quadrants represent the relashionship between unimanual left and unimanual right movement encoding. The simplest case, where contralateral and ipsilateral tuning functions are uncorrelated, generate high distance between them.

Table 3.2: Correspondence between condition number and movement direction for unimanual movements of the left and right hands in the RDMs.

Direction		0°	60°	120°	180°	240°	300°
Condition	Left Hand	1	2	3	4	5	6
	Right Hand	7	8	9	10	11	12

If there are tuning functions for unimanual movements, how are bimanual movements encoded? The simplest case is for us to assume that bimanual activity patterns will be a linear function of unimanual tuning (φ subscripts were dropped for clarity):

$$a(\theta_L, \theta_R) = a(\theta_L) + a(\theta_R) \tag{3.6}$$

Therefore, we can generate two separate components for bimanual left and bimanual right tuning. If both hands perform movements in N directions, there are N^2 combinations of movements. In a set of voxels which is exclusively left

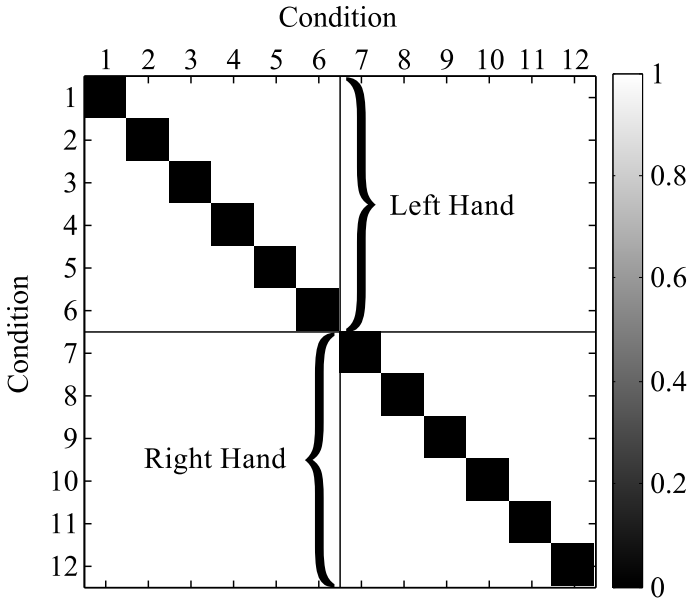

Figure 3.10: RDM for simulated patterns with narrow tuning function for left and right hands. Tested movements (θ) spanning from 0° to 300°.

hand tuned, only left hand movements will affect the RDM (Figure 3.11a). The same applies for right hand movements (Figure 3.11b). Each condition number in the RDM corresponds to the combination of a left and right hand direction, as shown in table Table 3.3.

Table 3.3: Correspondence between condition number and movement direction for unimanual movements of the left and right hands in the RDMs.

Direction	Left Hand	0°	0°	0°	0°	...	300°	300°	300°	300°
	Right Hand	0°	60°	120°	180°	...	120°	180°	240°	300°
Condition		1	2	3	4	...	33	34	35	36

If we assume the total distance to be separable, i.e., the overall distance for all conditions to be the sum of the previously shown components, we get the distance matrix shown in (Figure 3.12).

However, tuning functions might not be as narrow as a single voxel. If we simulate tuning functions as a Gaussian function centered on the preferred direction and width σ [88]:

$$a_{\theta,\varphi} = a + b \cdot exp\Big(-0.5\Big[\frac{\theta - \varphi}{\sigma}\Big]^2\Big) \tag{3.7}$$

Where a and b are constants which model offset and amplitude. The resulting RDM predicts that distances will increase away from the diagonal up to

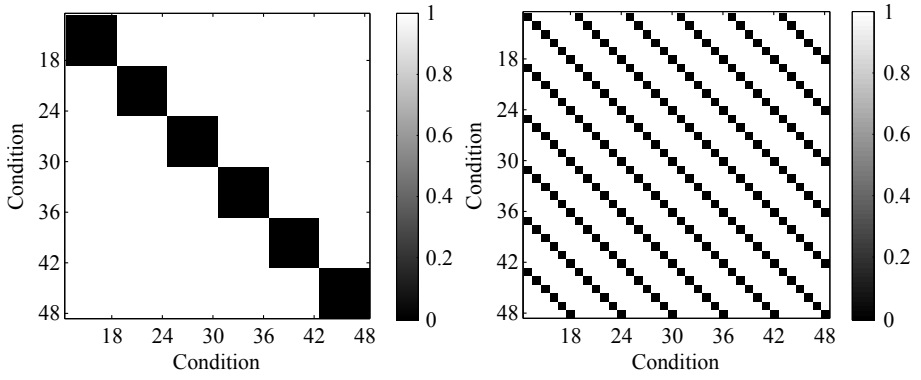

(a) (b)

Figure 3.11: RDMs for left **(a)** and right **(b)** hand movements for all bimanual combinations. Each of these RDMs are calculated from patterns based on the assumption of equation 3.6.

180°separation, and from that point they should decrease again. This effect can be observed in Figure 3.13.

Distance estimation

In the previous topic we simulated RDMs in order to predict how patterns of motor activity can be analysed using RSA. With fMRI data, we can use the $\hat{\beta}$ values from the GLM as patterns for each condition - but these patterns contain noise with spatial structure. This happens, for example, in voxels which have a nearby blood vessel. Such noise structure compromises reliability in the analysis [87].

In order to account for this effect, we can first estimate the variance-covariance matrix from the error term after GLM estimation (equation 2.2):

$$\hat{\Sigma} = \frac{1}{T}\epsilon^T\epsilon \tag{3.8}$$

And afterwards we perform multivariate normalization of the $\hat{\beta}$ values using $\hat{\Sigma}$:

$$\hat{U} = \hat{\beta}\hat{\Sigma}^{-1/2} \tag{3.9}$$

We will refer to this operation as pre-whitening.

If we calculate distances directly from these beta values, they will still be positively biased - so it is still not possible to infer directly on distance values. We can address this problem by cross-validating distances. If we have R repetitions of the experiment, i.e., R sessions, we can start by calculating the inner product using a modified version of equation (3.2).

$$\hat{G} = \frac{1}{R^2 - R}\sum_{a=1,b=1}^{a=R,b=R,a\neq b} U_a U_b^T \tag{3.10}$$

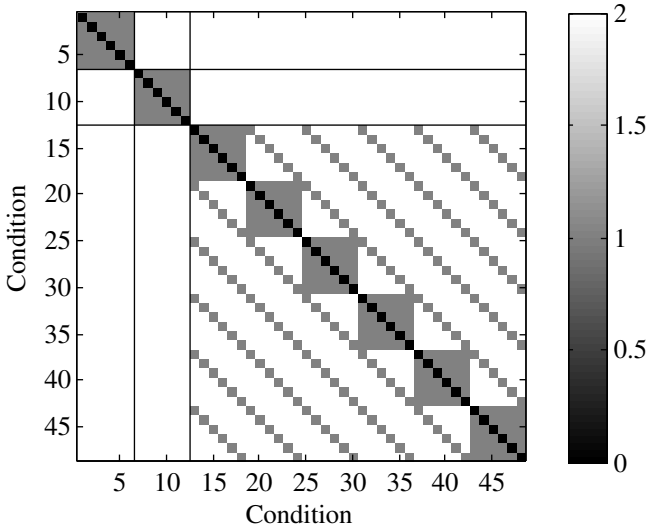

Figure 3.12: Simulated RDM for all conditions, obtained as a linear combination of the RDMs for unimanual and bimanual tuning functions.

where a and b iterate from 1 to R sessions. This is equivalent to split-half or leave-one-out cross-validation [87].

We then apply equation 3.3 to the estimated inner product matrix:

$$\hat{D}_{ii} = \hat{G}_{ii} + \hat{G}_{jj} - 2\hat{G}_{ij} \tag{3.11}$$

This computation was performed for all subjects independently, using the RSA toolbox [66, 82]. We obtained squared distance values in voxel space, cross-validated at session level. Because we expect *loci* of the motor system to encode movements differently from each other, RDMs where calculated for: primary motor cortex (M1), SMA, anterior and posterior SPL, PMv and PMd. Additionally, we extended this analysis to primary and secondary visual cortex (V12). ROIs were defined using Caret software - anatomical images were aligned to a template, and ROIs were obtained from pre-defined template regions adapted from Wiestler and Diedrichsen [89].

We also quantify directional tuning in unimanual left, right and bimanual cases. If there is no directional tuning, on average there will be no significant distance values. By assuming the distance matrices entries will be zero in this case, we can average the unimanual left, right and bimanual parts of the RDMs and test the hypothesis that these values are, on average, zero. Unimanual and bimanual parts are depicted in Figure E.1.

Bimanual tuning decomposition

The previous quantifications allows us to make inferences about unimanual contralateral and ipsilateral encoding. We are also able to test for encoding

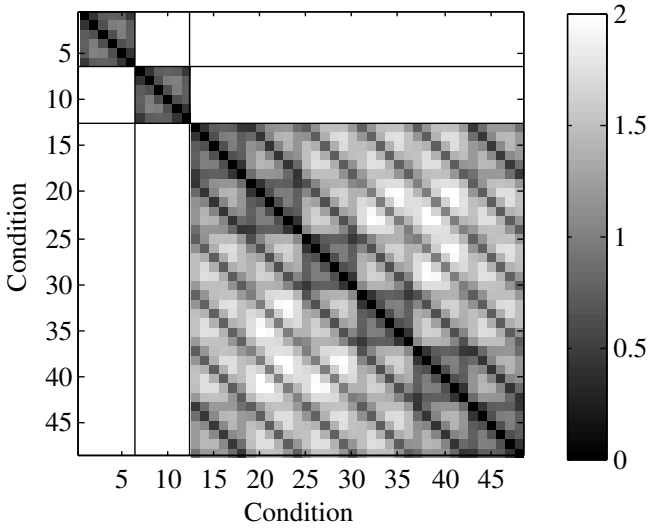

Figure 3.13: Simulated RDM for all conditions, obtained from patterns calculated according with equation 3.7, for a tuning width value of 30°.

during bimanual movements, but this effect may be due to the fact that either hand is moving - hiding possible effects of both hands and/or non-linear integration during bimanual movements. We futher investigate bimanual encoding by decomposing RDMs into distance tuning maps. We will now introduce the rationale for this decomposition.

If an ROI is encoding unimanual movements, we can estimate distance tuning functions by reorganizing the RDMs in terms of angle deviation. We start by redefining RDMs in terms of $\Delta\theta$ and align rows/columns in the RDMs. We then compute the average and estimate the unimanual tuning function of distance over $\Delta\theta$ as depicted in Figure 3.14.

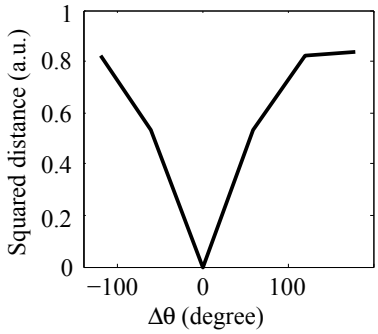

Figure 3.14: Unimanual tuning function derived from the RDM in Figure 3.13.

Similarly, we can reorganize the bimanual parts of the RDMs. Bimanual tuning functions can result from a linear combination of unimanual left and

right movements, or non-linear multiplicative combination. Bimanual tuning functions vary in both $\Delta\theta$ for the left hand and right hand, in such way that a purely left-hand tuned region would result in the tuning map show in Figure 3.15a, and for the right hand in Figure 3.15b. A region can also be tuned for both hands during bimanual movements in an additive or multiplicative (non-linear) manner. In the case of additive encoding, the resulting map corresponds to a linear combination of left and right tuning (Figure 3.15c). Alternatively, regions might encode movements of both hands non-linearly, which would result in Figure 3.15d.

We decomposed the bimanual RDM sections using the previously described method, with which we make qualitative observations on the nature of bimanual tuning (Chapter 5). Quantitative analysis using this method will be discussed in the scope of future work in Chapter 6.

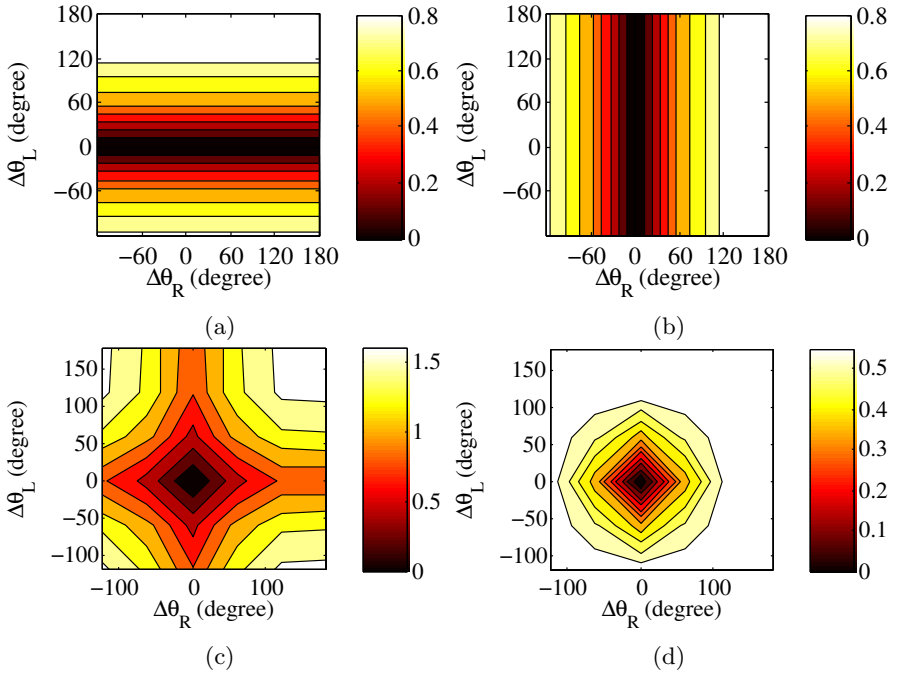

Figure 3.15: Bimanual tuning functions derived from a simulated RDM with bimanual left (**a**) and right hand tuning (**b**). Left and right can be combined into linear, additive tuning (**c**) and multiplicative tuning (**d**).

Chapter 4

Results

In this chapter we present the results of computations and statistical tests performed on behavioural/kinematics data and imaging data.

In summary, reaction times are not significantly different across unimanual or bimanual movements, directions nor hand combinations. Opposingly, there are significant effects on movement times across the previously referred conditions. Regarding imaging results, we present distance matrices for the tested movement conditions. We found strong contralateral and bimanual encoding across all regions, and strong ipsilateral encoding in most regions.

Details of these results can be found for behavioural/kinematics data in Section 4.1 and for imaging data in Section 4.2.

4.1 Behavioural

The questions posed in Section 3.6 were addressed in the upcoming sections. Section 4.1.1 presents the results from comparisons between unimanual and bimanual conditions with respect to RT and MT. At unimanual level, effects of direction in performance were tested in Section 4.1.2. At bimanual level, we tested effects dependent on directional relationship between both hands in Section 4.1.3.

Over these sections, conditions were compared individually for each subject, as each individual may behave distinctly from the others. This approach follows the same assumption of individuality as in RSA.

Additionally, conditions were compared within environments, i.e., within training and scanning settings. The motivation for comparing these populations separately for each setting are, on one hand, the environmental differences between training and scanning setups (loud MR scanner noise inexistant in training, room lighting, etc); and on the other hand, the visually evident bimodality in reaction time histograms when both training and testing data are overlayed (Appendix A, Figure A.1)

All datasets were confined to movements correctly executed, which account for $93\% \pm 5\%$ of the total number of trials in each subset.

4.1.1 Unimanual vs Bimanual

Boxplots for RTs and MTs during unimanual and bimanual conditions are presented in Figures 4.1 and 4.2. All data were tested for normality using the Kolmogorov-Sminorv test with $\alpha = 0.05$. Since all data subsets rejected the null hypothesis (that they come from a normal distribution), comparisons between unimanual and bimanual subsets were conducted using the non-parametric Mann-Whitney U test.

Figure 4.1 does not show visually pronounced differences between unimanual and bimanual conditions. Moreover some participants have higher bimanual RT median, whereas others have higher unimanual RT median. Only Subj.No. 3 and 7 have significant differences (marked with *) between these two conditions, as they rejected the null hypothesis that unimanual and bimanual RTs come from the same distribution (Mann-Whitney U test, $\alpha = 0.05$).

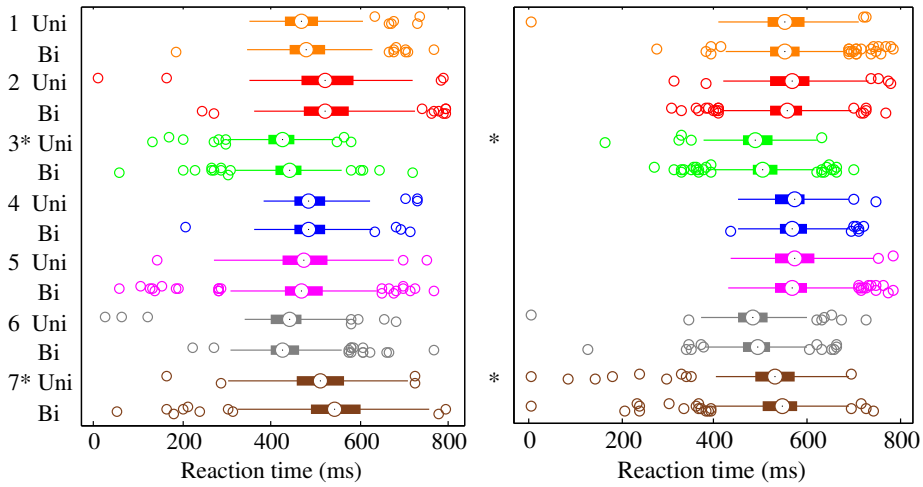

(a) Training (b) Scanning

Figure 4.1: Boxplots of reaction times in unimanual (Uni) and bimanual (Bi) for all subjects in *a*) training and *b*) testing sessions. Significant differences in reaction time between unimanual and bimanual conditions are marked by * ($\alpha = 0.05$, Mann Whitney U test). Neither population is normally distributed (Kolmogorov-Sminorv test, $\alpha = 0.05$).

Movement times were treated similarly to reaction times. Unlike RTs, MTs are visually different for unimanual and bimanual movements within each subject (Figure 4.2). Furthermore, bimanual movements involve longer MTs in all cases and this difference is always significant. Similarly to RTs, unimanual and bimanual MTs were compared using the Mann Whitney U test with $\alpha = 0.05$ after testing for normality.

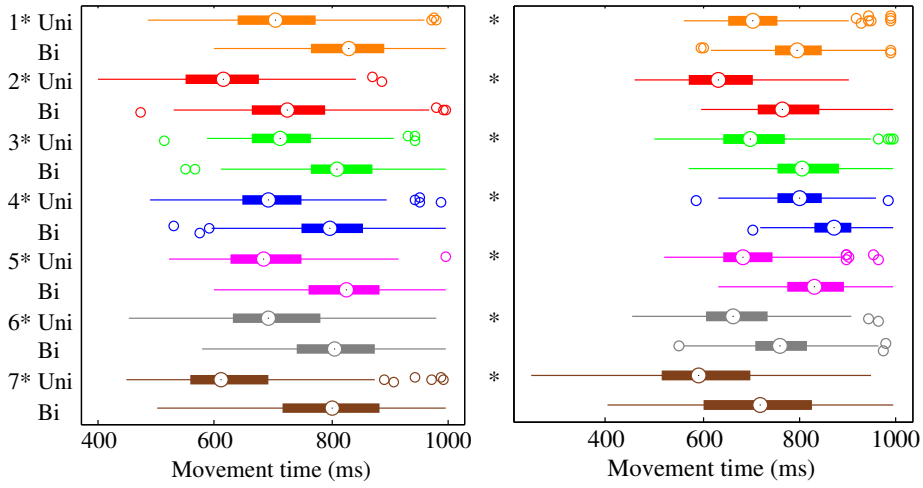

(a) Training (b) Scanning

Figure 4.2: Boxplots of movement times in unimanual (Uni) and bimanual (Bi) for all subjects in *a*) training and *b*) testing sessions. Significant differences in movement time between unimanual and bimanual conditions are marked by * ($\alpha = 0.05$, Mann Whitney U test). Neither population is normally distributed (Kolmogorov-Sminorv test, $\alpha = 0.05$).

4.1.2 Preferred directions

We searched for effects of direction in movements of either hand. Figure 4.3 shows radar plots of reaction times - for each direction, the median reaction time is represented.Because data is not normally distributed (Kolmogorov-Sminorv test, $\alpha = 0.05$), the non-parametric Kruskall-Wallis test was used to search for directional effects in RTs. Significance ($\alpha = 0.05$) is denoted by *.

Similarly to unimanual-bimanual comparisons, RT data does not account for a significant effect in most subjects, and significance is not always kept through training and scanning datasets (Figure 4.3).Only Subj. No. 2 shows significant and persisnt effect across hands and sessions.

Figure 4.4 represents MT data similarly to RT data in Figure 4.3. The Kruskall-Wallis test was also used in MT data, with $\alpha = 0.05$. The results are visually different from RT - left hand movements appear to have shorter MTs across the horizontal axis, particularly for the left hand (Figure 4.4).Significant effects are also present across a higher number of subjects than in RT results, particularly for the left hand (Figure 4.4).

4.1.3 Intrinsic vs Extrinsic vs Unrelated

Bimanual movements can be grouped in terms of the relationship of both hands. We defined **intrinsic** movements as combinations of mirror-symmetric hand movements; **extrinsic** as parallel combinations; and the remaining are **unrelated**. Figures 4.5 to 4.7 display boxplots of RTs, MTs and hand decoupling

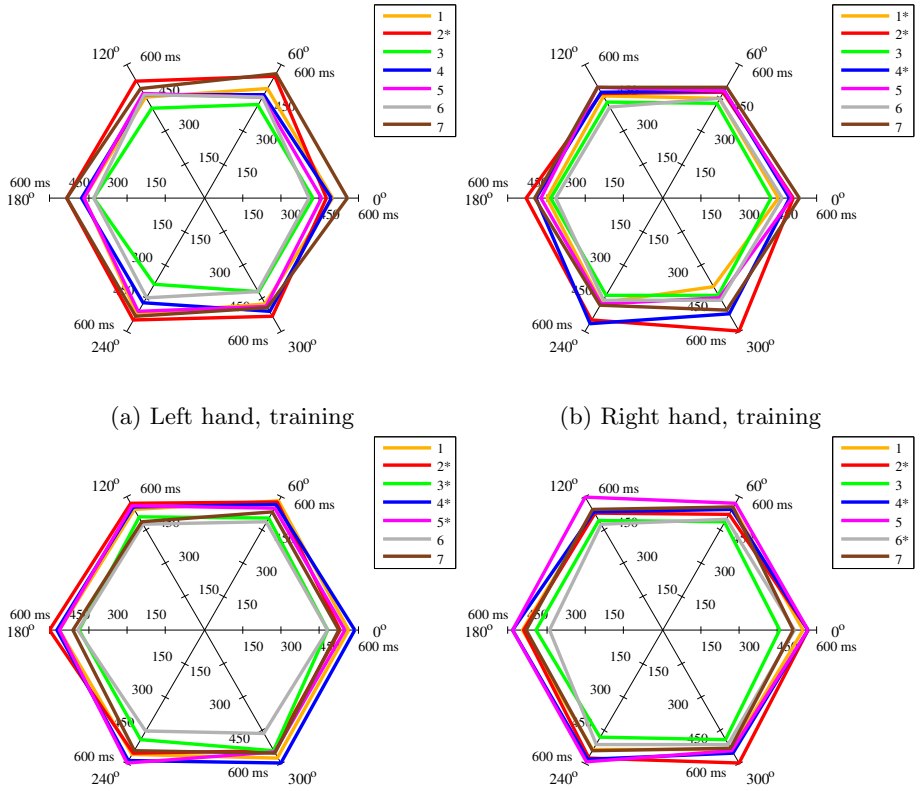

(a) Left hand, training

(b) Right hand, training

(c) Left hand, scanning

(d) Right hand, scanning

Figure 4.3: Radar plots of median reaction times for unimanual movement directions of all subjects, for the left (**a** and **c**) and right (**b** and **d**) hands. Significant effects of direction are marked by * (Kruskall-Wallis test, $\alpha = 0.05$)

for the training (left column) and scanning (right column) for all subjects.

The previous procedure for testing data for normality was applied. Kruskall-Wallis test results (significance for $\alpha = 0.05$ indicated by *) for RT are indicated in Figure 4.5. We applied this statistical test to check for effects of bimanual relationship in performance. Hand relationship does not account for effects in RT except for Subj. No. 3 in training and Subj. No. 7 in scanning sessions. Additionally, there is no consistence across testing and scanning results.

MT results are presented in Figure 4.6. All subjects except No. 7 have a significant effect of hand relationship in MTs. Moreover, significance is kept through training and testing results (Figures 4.6 **a** and **b**). The majority of subjects have lower **intrinsic** movement median MT than **extrinsic** or **unrelated**.

Bimanual movements were also analysed in terms of hand decoupling. As we can see in Figure 4.7 only subjects No. 1, 4 and 7 have significant hand relationship effects in decoupling, but significance is kept though training and

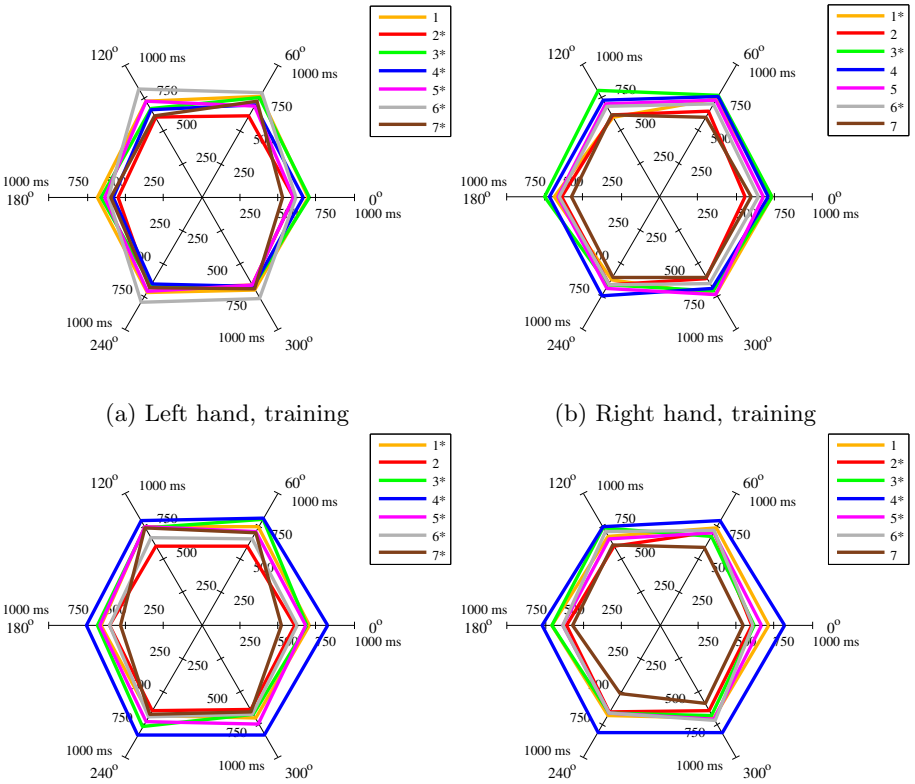

(a) Left hand, training

(b) Right hand, training

(c) Left hand, scanning

(d) Right hand, scanning

Figure 4.4: Radar plots of median movement times for unimanual movement directions of all subjects, for the left (**a** and **c**) and right (**b** and **d**) hands. Significant effects of direction are marked by "*" (Kruskall-Wallis test, $\alpha = 0.05$)

scanning sessions. However, the lowest RT median is not always associated with **intrinsic** movements, even in subjects with significant effects (Figures 4.7 **a** and **b**, Subj. No. 4 and 7).

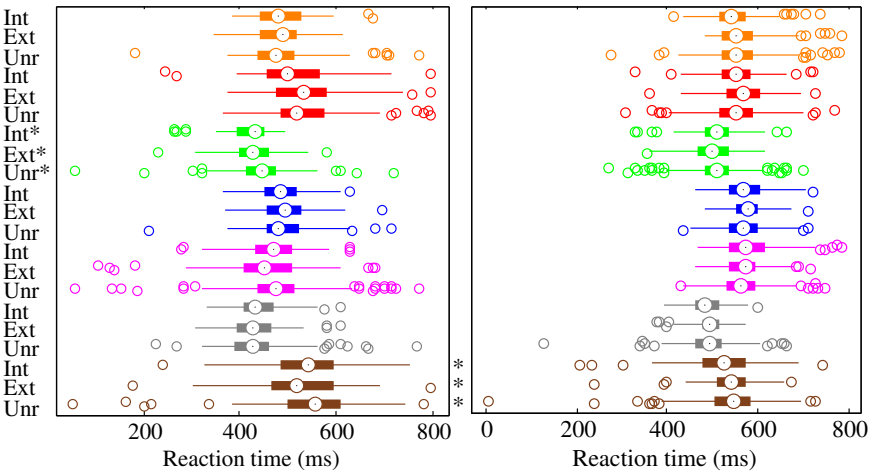

(a) Training (b) Scanning

Figure 4.5: Boxplots of reaction times in intrinsic (Int), extrinsic (Ext) and unrelated (Unr) for bimanual movements in a) training and b) scanning sessions. Significant effects in reaction time for movement categories are marked by * ($\alpha = 0.05$, Kruskall-Wallis test). Neither population is normally distributed (Kolmogorov-Sminorv test, $\alpha = 0.05$).

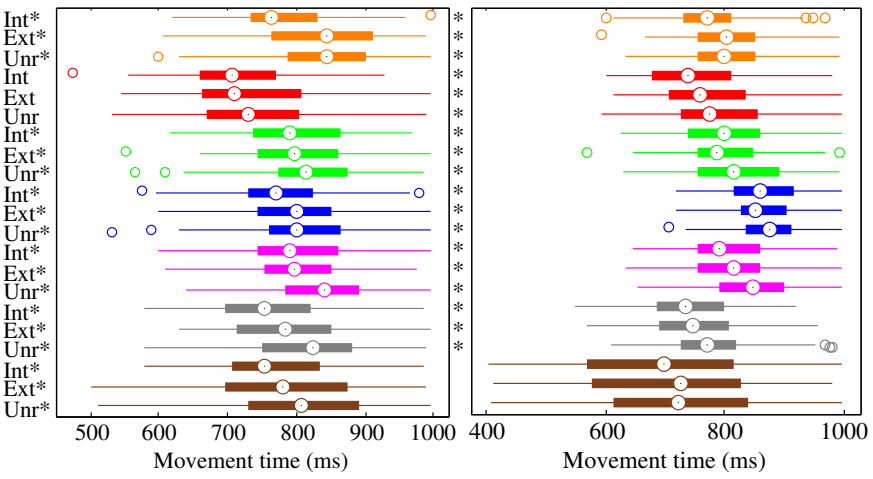

(a) Training (b) Scanning

Figure 4.6: Boxplots of movement times in intrinsic (Int), extrinsic (Ext) and unrelated (Unr) for bimanual movements in a) training and b) testing sessions. Significant effects in movement time for movement categories are marked by * ($\alpha = 0.05$, Kruskall-Wallis test). Neither population is normally distributed (Kolmogorov-Sminorv test, $\alpha = 0.05$).

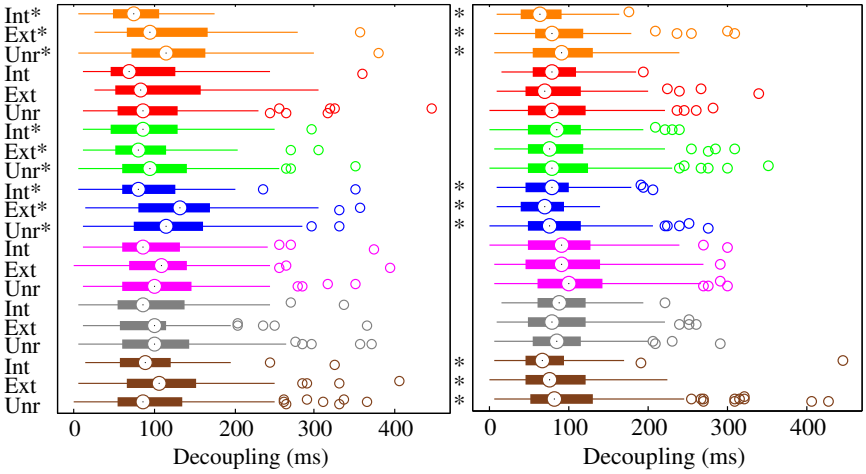

(a) Training (b) Scanning

Figure 4.7: Boxplots of decoupling (ms) in inrinsic (Uni), extrinsic (Ext) and unrelated (Unr) for all subjects in a) training and b) testing sessions. Significant differences in decoupling time between unimanual and bimanual conditions are marked by * ($\alpha = 0.05$, Kruskall-Wallis test). Neither population is normally distributed (Kolmogorov-Sminorv test, $\alpha = 0.05$).

4.2 Imaging

After comparing movement conditions with respect to kinematic performance (Section 4.1), we now focus on analysing them with respect to functional activation in MRI. We start by localizing activation correlates using a classical univariate method (Section 4.2.1). Afterwards we present the results of RSA (Section 4.2.2), find which brain regions encode movement (Section 4.2.3), and present unimanual and bimanual tuning functions (Section 4.2.4).

4.2.1 Hand movement localization

We can visualize activation areas for each subject by looking at contrast maps. Univariate contrast maps for unimanual left, unimanual right, and bimanual movements for each subject are shown in Appendix C, Figures C.1 to C.7. These maps result from computing t-Contrasts for the β values obtained as output from SPM software, as described in section Section 3.7.1. Images contain contrasts mapped onto a 3D cortical surface using Freesurfer and Caret for ROI identification.

Contrast maps like these allow us to identify which brain regions are active during certain conditions.

We can use the cortical segmentation in Caret, derived from a cortical atlas, to visually inspect these results. There is, across all subjects, higher activation during contralateral movements than ipsilateral movements. Bimanual movements, on the other hand, have much higher and widespread activation than unimanual movements.

It is also noteworthy that activation is not fully similar, both in value and *loci*, across subjects, i.e., there is inter-subject variation in activation *foci*.

Given the high inter-subject variability, we quantified activation individually for each subjecct in the following ROIs, for both hemispheres: S1, M1, PMv and PMd, SMA, V12, SPLa and SPLp. Results are show in Appendix D, Figures D.1 to D.7.

4.2.2 Representation Dissimilarity Matrices

The previous section shows results for activation/localization, but they do not tell us about encoding/tuning. The results in Figure 4.8 show the RDMs for the S1 and M1 regions averaged across all subjects using the methodology in Section 3.7.2. Results for the remaining ROIs can be found in Appendix F, Figure F.1.

This measure of encoding is adimensional (average of dissimilarity values). Inter-subject correlations can be found in appendix G.

In the RDMs, each value is a cross-validated pairwise comparison between conditions. By observing left and right hemispheres, we can observe that the high distance values between ipsilateral and bimanual movements stand out

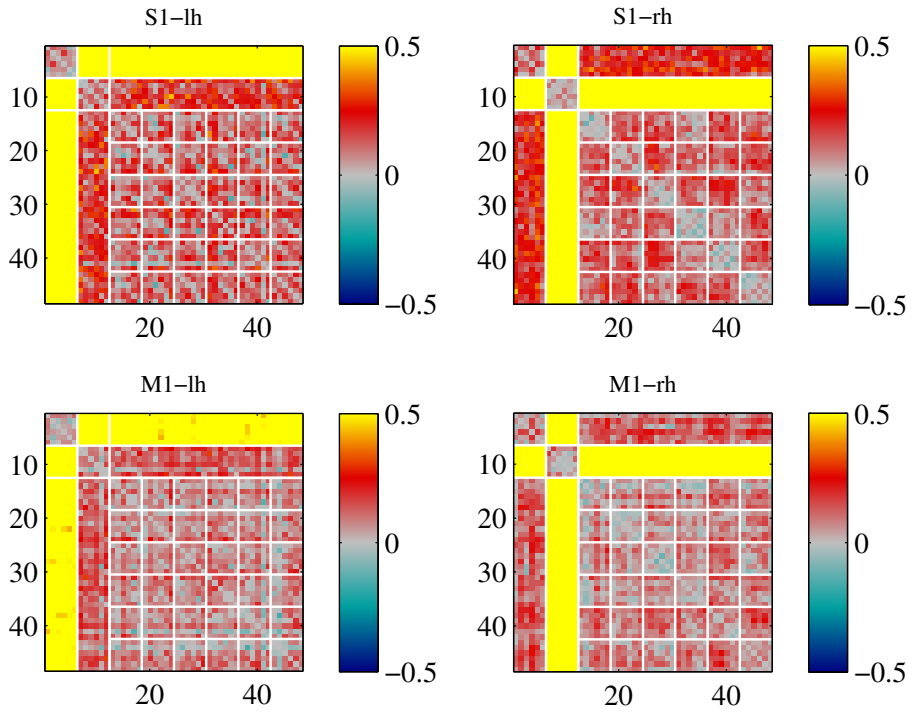

Figure 4.8: RDMs averaged across all Full Study Subjects for the S1 and M1 regions in the left and right hemispheres. Each value in the RDMs is the squared distance in voxel space, between every two conditions (arbitrary units).

(Figures 4.8 and F.1, see Figure E.1 for RDM sections). Furthermore, ipsilateral and contralateral movements are highly dissimilar across all ROI's. Directional tuning also appears to be present for contra and ipsilateral movements in all ROI's, event though tuning structure is encoded with different strength and width across regions.

4.2.3 Contralateral, Ipsilateral and Bimanual encoding

Visual inspection of the RDMs provides quantitative pairwise information and qualitative information about encoding/tuning structure. However, we can quantify contralateral, ipsilateral and bimanual encoding by taking distance values in certain parts of the RDMs and testing this difference for zero median as an estimate of encoding.

Results can be found in Figure 4.9, methods in Section 3.7.2, and RDM sections in Figure E.1. This evaluation is based on the assumption that distance values will be zero if the true distance between conditions is zero. We further confirmed this assumption by randomizing condition labels.

Furthermore, we can ask if a certain region encodes Contralateral movements more or less strongly than Ipsilateral movements. If Contralateral and Ipsilateral

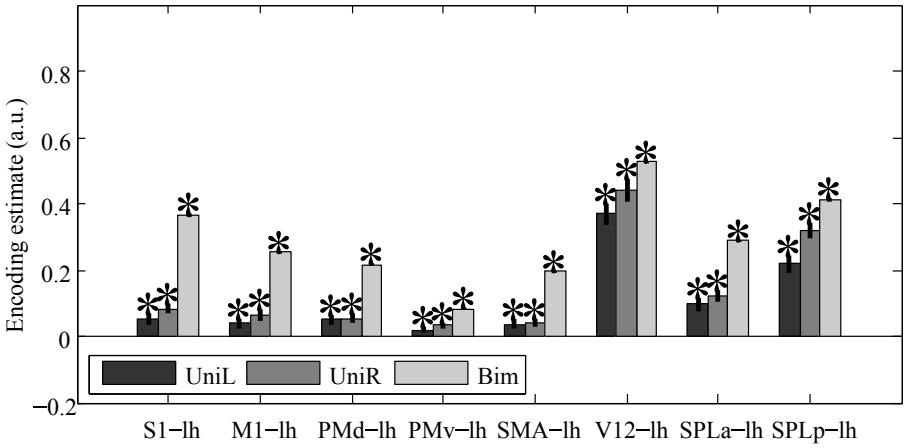

(a)

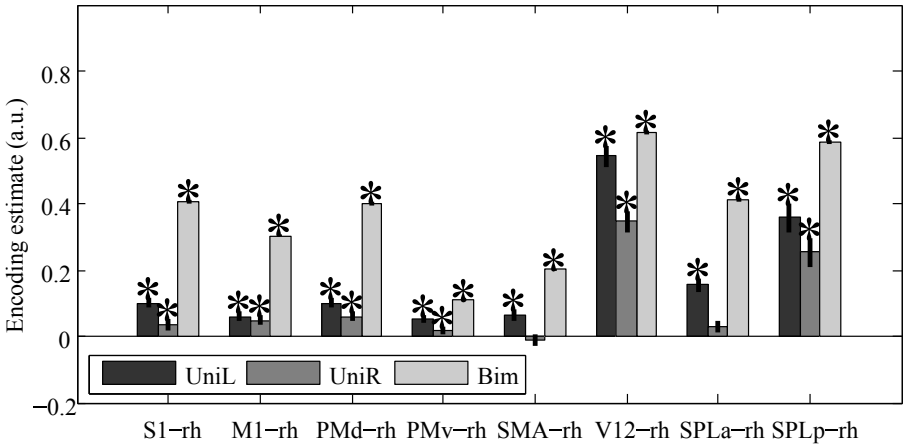

(b)

Figure 4.9: Unimanual Left, Right and Bimanual estimate of encoding for each ROI in the left (**a**) and right (**b**) hemispheres, averaged across all subjects. Values obtained by averaging distance values in the RDMs. Significance indicated by *, One-Sample Wilcoxon Signed-Rank Test, $\alpha = 0.05$.

movements are encoded differently, we can test for differences in Unimanual Left and Right distance values with the Mann-Whitney U-test. Table 4.1 contains the p-values for a two-sided Mann-Whitney U test of contralateral and ipsilateral encoding in all tested ROI's.

Table 4.1: P-values for tested differences between Contralateral and Ipsilateral tuning. Mann-Whitney U test. Highlighted p-values indicate significance, $\alpha = 0.05$.

	LH	RH
S1	0.1618	**0.0030**
M1	0.1847	0.5014
PMd	0.9240	0.1473
PMv	0.4660	0.1386
SMA	0.7231	**0.0020**
V12	**0.0379**	**6.1641e-05**
SPLa	0.2133	**3.5207e-06**
SPLp	0.1645	0.1737

4.2.4 Bimanual tuning functions

In order to extract bimanual tuning maps, we can reorganize distance values in terms of angle difference for the left ($\Delta\theta_L$) and right ($\Delta\theta_R$) hand directions. Bimanual tuning can simply arise when left hand movements, for example, are being executed - left hand tuned neurons/voxels will respond the same way regardless of movements being unimanual or bimanual. In this case, bimanual encoding values will be significant, but they could be explained by left hand movements alone. This scenario would predict the result in Figure 3.15a, and similarly for right hand movements in Figure 3.15b.

Bimanual tuning maps could, however, take different shapes if voxel responses combine them in a linear (Figure 3.15c) or non-linear manner (Figure 3.15d).

In this section we show the results for bimanual tuning maps in left and right hemisphere ROIs. Figure 4.10 shows bimanual tuning maps for S1 and M1.

Results for the remaining ROIs can be found in Appendix H, Figure H.1. The majority of ROIs strongly resembles bimanual tuning associated with the contralateral hand, when compared with the maps obtained by simulation (Figure 3.15). Some ROIs, however, have tuning maps varying with both left and right hand directions, such as SMA and PMv.

Bimanual tuning maps will be qualitatively discussed in Chapter 5.

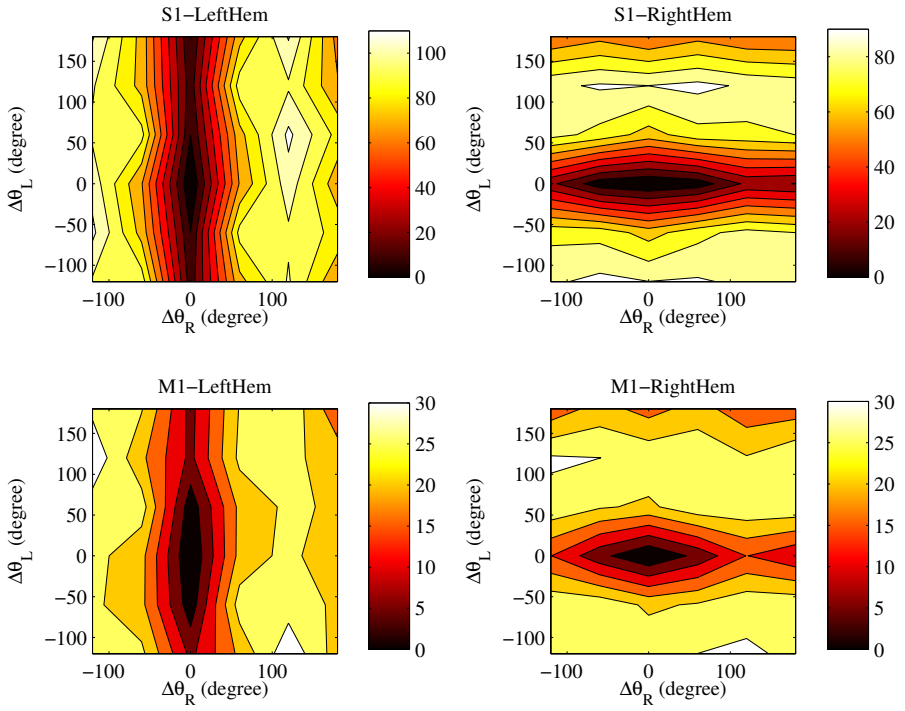

Figure 4.10: Bimanual tuning maps for M1 and S1, obtained by re-organizing the RDMs and averaging squared distance values (arbitrary units, distance before normalization by number of voxels). Left and Right hemispheres on left and right side of figure, respectively.

Chapter 5

Discussion

5.1 Behavioural

Kinematic analysis in this project was conducted individually for each subject, in order to account for different motor performances. Moreover, we separated training and testing subsets, due to the discrepancy between a quiet training room and a constrained loud MRI room. We illustrate the performance difference between environments by showing histograms of reaction time for one subject in Figure A.1. Significant differences were found between environments, both in unimanual and bimanual movements.

We might consider that performance is different in training and scanning setups because subjects are more experienced after training. However, that hypothesis would predict that reaction times would be shorter in training environment, but we observe the opposite. Moreover, no learning effects were observed over time due to task simplicity. Participants were allowed to experience the task before data acquisition, as part of instructing them - purposely discarding learning effects.

5.1.1 Unimanual vs Bimanual

With the exception of Subjs. No. 3 and 7, RT does not predict whether movements are unimanual or bimanual (Figure 4.1). For the remaining subjects, RTs are not even consistently higher in bimanual movements than unimanual ones. We might expect slower reaction to bimanual movements due to higher number of targets and limbs to control. However, subjects were prompted with the targets 2 seconds before movement onset, which provides time for movement planning. In fact, bimanual RT discrepancy is eliminated when direct visual cues are presented, which might be a consequence of bimanual interference associated with the duration of movement planning for generation of complex motor commands [38].

Unlike RTs, MTs are consistently higher in bimanual movements than unimanual, across all subjects and environments (Figure 4.2). This finding suggests

that bimanual movements are harder to execute. During bimanual movements, the motor system is required to synchronize both hands and direct them accurately towards two targets instead of one. Speed-accuracy tradeoff is a well-known effect in motor behaviour, consisting of degrading performance when speed is increased, and vice-versa (model review in [90]). Even though speed-accuracy studies typically concern unimanual movements, it might be possible that controlling two hands accurately takes more time (less speed).

5.1.2 Preferred directions

We also analysed, in terms of RT and MT, the effects of directions during unimanual movements (Figures 4.3 and 4.4). In these figures, we display the median, rather than the mean of each subject, because it better represents a skewed population, and because it is the value presented in the center of boxplots. This way the median is a representative value of the populations we study across kinematics data.

Except for subject No. 2, RT differences do not seem to be explained by direction (Figure 4.3). For the remaining subjects, directional effects in RT are not consistent across hands not sessions, except for Subj. No. 4, right hand. Therefore, we cannot conclude RT has a strong directional effect. Again, this might be explained by the fact that movements are visually cued before onset [38]. However, further research should be conducted to test for any muscular constraints at subject level that, despite not observed in our study, might be associated with wrist pronation/supination.

We also tested for directional effects in MTs similarly to RTs (Figure 4.4). These effects are more frequent than RT, particularly for Subjs. No. 3 and 6 who present strong directional effects. The remaining subjects are not always coherently sensitive to direction across hands nor sessions. Movements along the horizontal axis (0° and 180°) seem to be associated with shorter MTs. However, the reason might not have neural origin - instead, these movements could be simply associated with wrist flexion movements being more easily performed than ulnar deviation. This hypothesis could be tested in the future by rotating the device in a similar manner to the work of Kakei et al., or by analysing natural movement statistics, relating them to daily hand usage [28].

5.1.3 Intrinsic vs Extrinsic vs Unrelated

Another question we were interested in regards the influence of hand relationship in bimanual movement performance. We split out bimanual data into intrinsic (mirror-symmetric), extrinsic (parallel) and unrelated (all the remaining ones) movements.

As shown in Figure 4.5, hand relationship does not have an effect in reaction time. This is something we would also expect directly from providing visual cues [38]. MTs, however, are consistently sensitive to hand relationship, with the exception of Subj. No. 7 during scanning sessions Figure 4.6. Intrinsic

combinations frequently have lower MTs than parallel and unrelated, suggesting that performing these movements is easier. Moreover, parallel movements are often associated with lower MTs than unrelated. We would actually expect these effects to be present, and it should be a direct consequence of bimanual interference. Such effects have been observed before, and suggest that neural control of bimanual movements is sensitive to parameters of both hands, implying inter-hemispheric cross talk [35, 36].

Given the previous conclusions, we would expect hands to be more tightly coupled during intrinsic movements than parallel or unrelated. We added the time difference at the beginning and end of each hand movement and used it as a measure of decoupling (Figure 4.5). However, except from Subjs. No. 1 and 4, no consistent effects were observed. It might be possible that our measure of decoupling is not sensitive enough to reveal an effect, because it measures two timepoints rather than accompanying the hands over the whole trajectories.

5.2 Imaging

5.2.1 Hand movement localization

The univariate contrast maps displayed in Figures C.1 to C.7 show T-statistic values for each voxel. These T-values are the result of computing the t-statistic at each voxel for the conditions in study (unimanual Left, Right or bimanual) against the resting baseline - and hold negative or positive values according with β value correlation with the condition in study. Each activation value is calculated as a β weight of the HRF regressor - in a way that activation values in fMRI do not represent neuronal activation *per se*, but rather correlates of the hemodynamic response. Inter-subject variability can be associated not only with neurological variables, but may also have physiological origin (blood perfusion, for example) [58].

Commonly across all subjects, we find significant activation in nearly the whole cortical surface. Contralateral movements appear to be associated with higher activation than ipsilateral ones, as would be predicted by the classical view of contralateral movement control. Despite weak, ipsilateral activation is also present. Yet, this does not tell us whether there is directional encoding or not.

Bimanual movements seem to activate both hemispheres similarly in both hemispheres and more significantly than in unimanual cases. However, we cannot directly compare T-values in unimanual and bimanual conditions because higher bimanual T-values might associated with higher number of bimanual conditions, relative to unimanual ones.

Instead, we can get this information from the β values in each ROI by averaging them and testing the mean against zero (Figures D.1 to D.7).

Ipsilateral activation is typically lower than contralateral and bimanual, as expected, and not always significantly different from zero. Some regions activate more during unimanual than bimanual movements, suggesting their preference

for bimanual movements. This effect appears to be more frequent in regions hierarchically closer to muscles such as S1 or M1. Opposingly, premotor areas which are though to be associated with movement planning and abstract movement representations are more highly activated during bimanual movements.

These values, however, will tell us whether a certain region activation is, on average, positively, negatively or non correlated with the condition in study. Similarly to the contrast maps, we find high inter-subject variability. Moreover, there is no consistent average activation across ROIs - some subjects have higher PM activation whereas other have higher S1 or M1 activation. V12 is an important example, as some subjects have low (non-significant) activation (Figures D.3 and D.5) or even negative (Figure D.6).

Even though we can quantify activation at every voxel for all conditions, this does not mean active voxels encode a certain condition. For example, if a certain voxel is always equally active for left hand movements, we would not be able to decode directional information from it. Moreover, because activation sites are not exactly the same for all subjects, averaging activation values for each voxel across all subjects would tell us which areas are commonly recruited across a population, but fine subject-specific variations, possibly important for motor encoding, would average towards non-significant values, causing us to loose important information.

This is part of our motivation to complement univariate analysis with multivariate pattern analysis - where we assume that the overall relationship between conditions will be the same for every individual, but each subject may have specific encoding patterns. Therefore, we focus on the common structure of representation rather than average activation.

5.2.2 Representational Dissimilarity Matrices

Pairwise comparisons between conditions can be found in Figures 4.8 and F.1. These figures contain RDMs averaged across all subjects, and generally, higher distance values are indicative of stronger encoding. Within-subject correlations can be found in Appendix G, Figure G.1.

In both hemispheres and across all ROIs, directional tuning appears to be present. In fact, directional tuning has been found in all motor regions where it has been sough for [24]. However, its structure has not yet been fully characterized.

We start by analysing unimanual contralateral parts of the RDMs, i.e., *UL* for ROIs in the left hemisphere, and *UR* in the right hemisphere (Figure E.1). Directional tuning is clearly present, though with different strength and width. Interestingly, ipsilateral tuning also appears to be present in almost all ROIs. The presence of ipsilateral encoding once again challenges the classical view of contralateral control, and presents a clear structure, similarly to recent findings [4, 5].

Unimanual tuning, both for left and right hands, appears to have larger width in regions such as S1 and M1, when compared to V12 or SPLp (Figures 4.8 and F.1, simulations in Figures 3.12 and 3.13, RDM sections in Fig-

ure E.1). Narrower tuning functions don't imply better encoding *per se*, but can be a consequence of higher innervation. Tuning width is also known to depend on task directional accuracy, e.g., tasks with closer targets would generate narrower tuning functions [24]. In this sense, it is possible that lower-level motor areas such as M1 are more sensitive to task accuracy for modulation of tuning functions.

The RDM sections that stand out the most are clearly the *Contra* & *Ipsi* and *Ipsi* & *Bimanual* (for ROIs in the left hemisphere this corresponds to *UL* & *Bimanual*). The fact that contralateral and ipsilateral tuning is highly dissimilar suggests that each hemisphere codes for movements of both hands differently. Since the patterns for contralateral and ipsilateral tuning are different but exist in the same neural representational space, they can be though of as representational maps rotated from each other in neural space [63].

Moreover, bimanual tuning is highly dissimilar from ipsilateral tuning, but not from contralateral tuning (Left and Right S1 and M1). This suggests that there bimanual tuning might derive from contralateral tuning. However, because we are estimating the Euclidean distance in representational space, our measure might also be capturing differences in the vector norm caused by lower ipsilateral activation. We will address this question in the future.

Bimanual tuning is also strongly present across the cortex, particularly in V12, anterior and posterior SPL, S1 and M1. In particular, bimanual tuning structure in V12 strongly resembles simulated bimanual left and right components (Figures 3.11a and 3.11b). We have not yet developed a suitable decomposition of the bimanual component, but this question will be adressed in the future.

Future work for our multivariate approach might also involve relating behavioural data with RDMs. One way of doing this might be to include reaction and movement times in the general linear model as confound regressors - influencing our β regressors of interest (condition-specific).

5.2.3 Contralateral, Ipsilateral and Bimanual enconding

In this section, we quantify movement encoding by taking the average of contralateral, ipsilateral and bimanual parts of the RDMs for each ROI (results in Figure 4.9).

As expected, we found significant contralateral enconding in all ROIs. More interestingly, we find significant ipsilateral encoding in all ROIs in the left hemisphere, and most ROIs in the right hemisphere, matching resent results where strong ipsilateral representations were found [4, 5].

Bimanual encoding is always stronger than unimanual in all ROI's. In the simplest case, bimanual movements are composed by a linear combination of bimanual ones, which would predict that it is at least as strong as unimanual components.

Contralateral encoding is significant across all ROI's, unlike ipsilateral, which is not significant in right SMA and SPLa. We further investigated differences

between contralateral and ipsilateral encoding (Table 4.1), revealing that the right hemisphere has significantly weaker ipsilateral tuning than the left hemisphere. Given that the right hemisphere is the non-dominant, these findings suggest that the non-dominant hemisphere is more specialized in the sense that it encodes contralateral movements preferentially.

Such quantification provides a useful estimate of how strongly directions are encoded in each ROI. Because we simply take the average, we don't force a specific tuning function shape. Instead we only rely on assumption that absence of encoding will lead to zero distance. We confirmed this by randomizing condition labels on real data, which resulted in zero-distance RDMs. However, we should point out that the average distance computation is sensitive to the tuning width (see contralateral M1 and SPLp response, Figure 4.9) - wider tuning functions will lead to distance values which decrease gradually after 180° difference (M1 and S1 RDMs, Figure 4.8).

5.2.4 Bimanual tuning functions

Future steps in this project will involve decomposing bimanual tuning and test its relationship to unimanual tuning. We can reorganize RDMs into tuning functions of representational distance over angle difference ($\Delta\theta$), as simulated in 3.15. From these figures, we can visualize what the structure of a left or right hand tuned ROI is like - it varies only along the directions of the arm it encodes for. Alternatively, ROIs may encode for both hands linearly or non-linearly.

If we apply this computation for the bimanual parts of the RDMs, we obtain the results shown in Figure H.1. We can qualitatively compare these tuning functions with the ones simulated in Figure 3.15. Most ROIs in the left and right hemispheres appear to have bimanual tuning strongly related to contralateral tuning. However, right SMA and PMv resemble non-linear encoding as simulated in Figure 3.15, suggesting these regions might play a specialized role in bimanual control. If an ROI encodes directions of left and right hand non-linearly, that ROI is coding for bimanual movements in a specialized manner and this mechanism may be important for bimanual coordination.

Even though we have not yet conducted a quantitative evaluation of linear and non-linear tuning - and consequently cannot evaluate how significant each encoding type is - these results motivate us to look further into this question. Future steps will involve quantitative evaluation of linear/non-linear components for modelling bimanual tuning from the RDMs.

Chapter 6

Conclusions and Future work

In this thesis, we investigate directional tuning in unimanual and bimanual movements using novel techniques. For the most part, we find clear differences in unimanual and bimanual performance, particularly in movement times. Directional effects are also present in unimanual movements. However, these are not fully consistent across all subjects, and the cause for them should be revisited by examining daily behaviour where wrist directions vary. One interesting approach would be to monitor wrist movement frequency in everyday task over each direction and relate it to reaction and movement time performance in our study.

We would also expect bimanual movements to be highly different across intrinsic, extrinsic and unrelated combinations. However, our findings suggest except for movement times, reaction times and synchronization between hands are not related to these combinations. One possible explanation is that movements in this project were simple and did not involve quick cyclic repetition, in which case we would expect intrinsic movements to out-perform extrinsic and unrelated ones [36].

The image analysis methods used in this work were based on novel fMRI analysis. Using multivoxel pattern analysis allows us to look for the structure of directional movements and compare it with simulated results based on previous tuning function definitions [7]. Similarly to previous studies, we find directional tuning in all tested regions [24]. Contralateral tuning is present in all ROI's, as predicted by the classical view in motor control. However, we also find strong ipsilateral representations - also present in recent studies at arm and finger movements [4, 5].

Bimanual movement encoding, like unimanual movements also seems to be present strongly across all ROI's. However, the presence of bimanual tuning can be explained simply because corresponding unimanual movements are being executed, i.e., bimanual representations might result from linear integration of unimanual movements. Nevertheless, controlling both hands simultaneously in

highly coordinated movements, such as tying laces or playing the piano, might benefit from a multiplicative encoding scheme where bimanual tuning functions result from specific combinations of unimanual components. We cannot yet quantify how much bimanual tuning is explained by additive or multiplicative tuning, but we hope to address this question in the future.

Further analysis on this dataset should be conducted in order to quantify each type of bimanual encoding. Particularly, relating simulated bimanual encoding results with results from real data in regression models might be key to answer this question.

One issue with ROI analysis is the selection bias it implies: because analysis in conducted in priorly specified regions, areas outside those regions are ignored. Furthermore, the specification of an ROI does not account for small variations within the region which might be otherwise evident in smaller area specifications. One approach which would complement our methods is searchlight analysis. This method consists of conducting our multivoxel pattern analysis in a small spherical ROI which iterates over the cortical surface. Using this approach would not only increase the cortical area we analyse, but would also allow us to obtain continuous encoding maps, analogous to t-contrast maps obtained in univariate analysis.

Besides analysis methods, experiment tools could also benefit from improvement. Future studies might benefit from revisiting the wrist device structure to achieve more comfortable and natural positions. More importantly, sensors and device-sensor coupling should be improved. Despite accurate, resistive-surface encoders wear out very quickly, forcing us to replace them frequently. A suitable MR-compatible alternative would be optical rotation encoders.

Regarding the experiment design, one alternative to using wide wrist range of movements would be imposing force fields and having subjects countering them. This approach would not only mitigate problems associated with movement range in the MR scanner, but would also allow controlling the experiment difficulty more easily by modulating force amplitude and direction.

Regardless of the methods used, the experiment could be improved by increasing the population sample beyond 7 subjects, which was not possible due to time constraints.

Despite the issues and future improvements to be made, our results match recent findings, and challenge old ones. Knowledge about the structure of movement encoding might be key in future clinical applications for movement impairments and disorders. Characterizing the motor system in healthy and pathological cases might be particularly useful as a way of evaluating the progress of rehabilitation therapy methods, and it might provide a framework for active control of neuroprosthetic devices.

Appendix A

Bimodal distribution

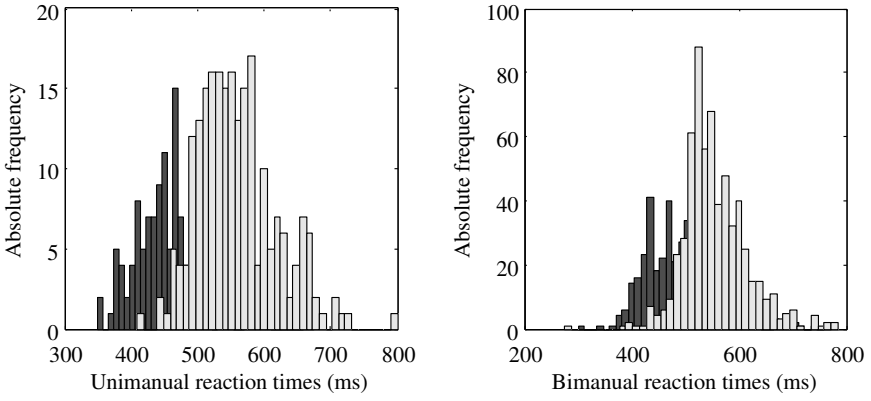

(a) Unimanual (b) Bimanual

Figure A.1: Histograms of reactions times of Subj.No. 1 during unimanual (**a**) and bimanual (**b**) movements. Training data (dark grey) overlayed by scanning data (light grey). **a)** Neither training nor scanning reaction times are normally distributed (Kolmogorov-Sminorv test, $\alpha = 0.05$). Within unimanual and bimanual RT's, training and testing sets come from different distributions (Mann-Whitney U test, unimanual set: $p = 1 \cdot 10^{-32}$; bimanual set: $p = 1 \cdot 10^{-63}$).

Appendix B

Cortical regions

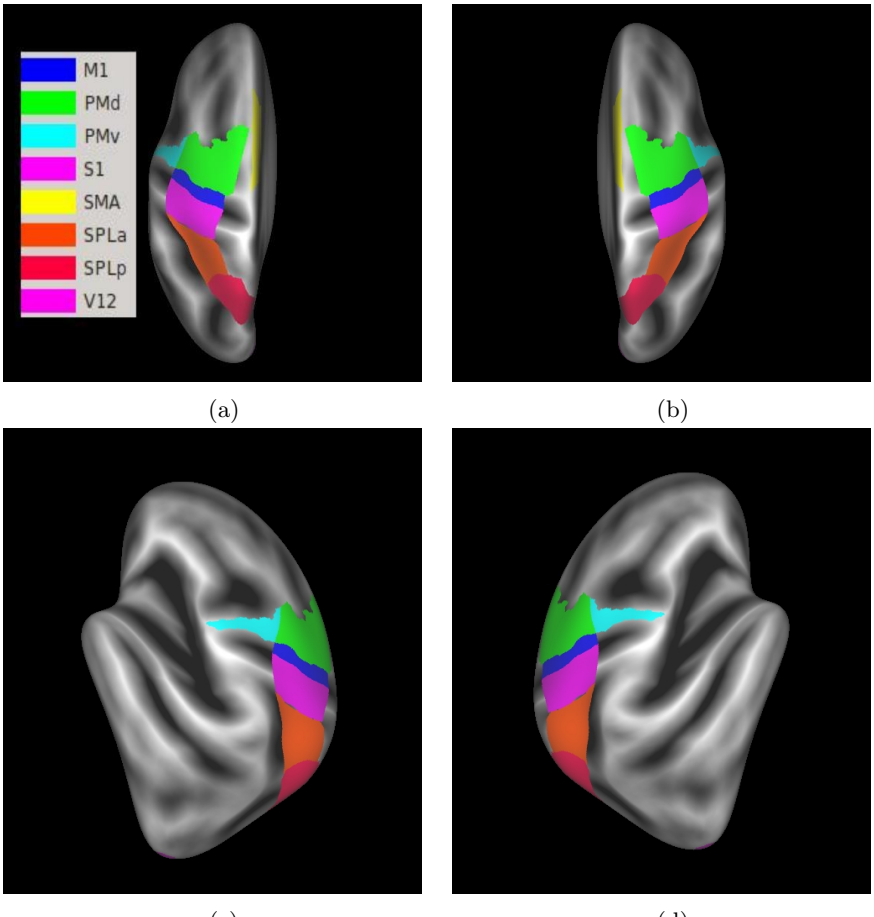

(a) (b)

(c) (d)

Figure B.1: Regions of Interest (ROI) adapted from reference [89] overlayed on *fsaverage_sym* template.

Appendix C

Univariate contrast maps - Full Study

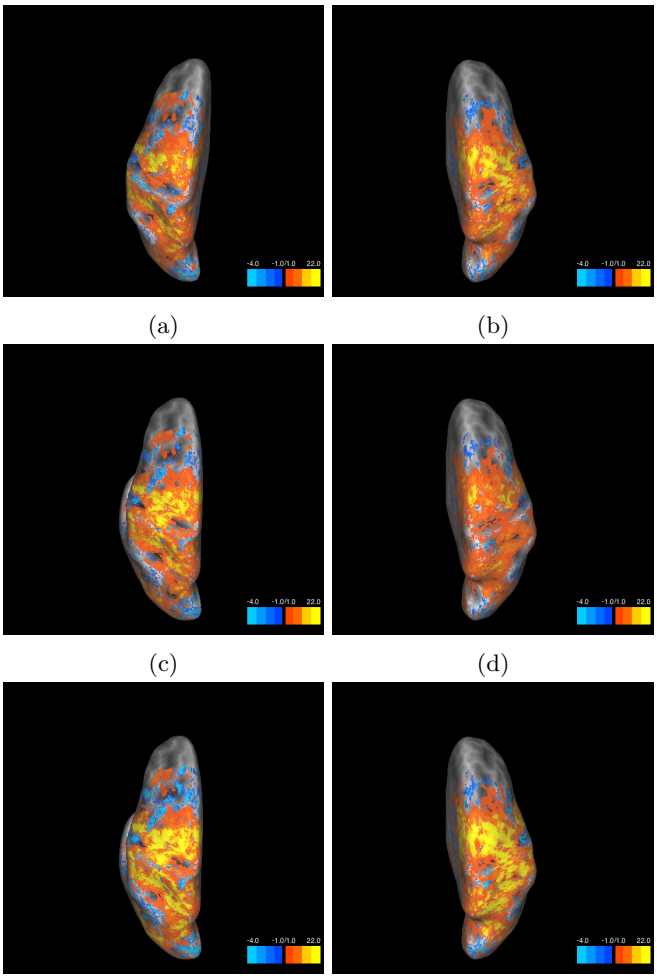

(a) (b)

(c) (d)

(e) (f)

Figure C.1: t-Contrast maps for unimanual left, unimanual right and bimanual movements for the Left and Right Hemispheres, Subj.No 1.

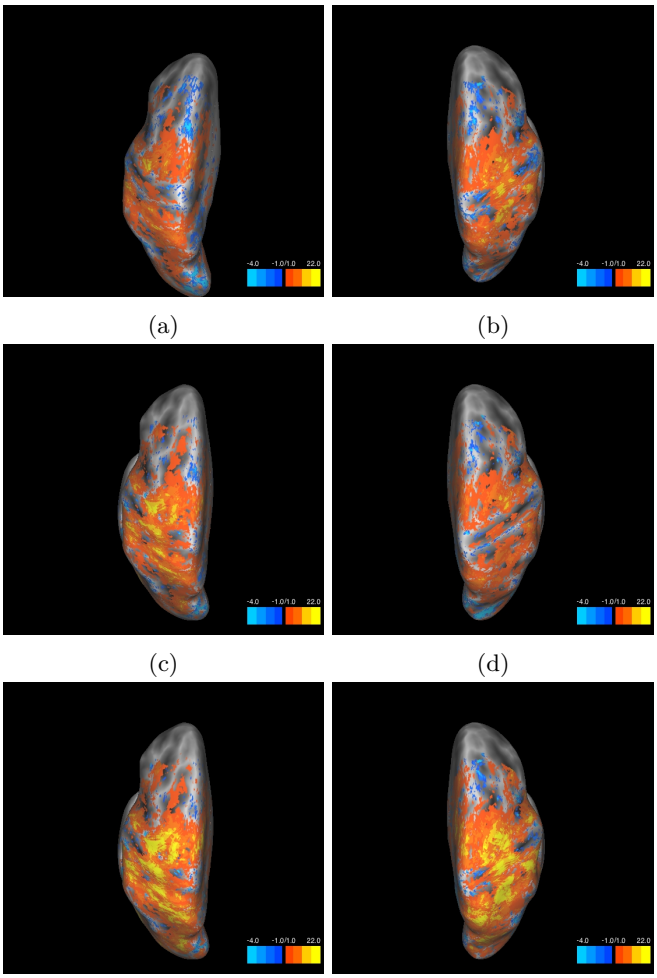

(a) (b) (c) (d) (e) (f)

Figure C.2: t-Contrast maps for unimanual left, unimanual right and bimanual movements for the Left and Right Hemispheres, Subj.No 2.

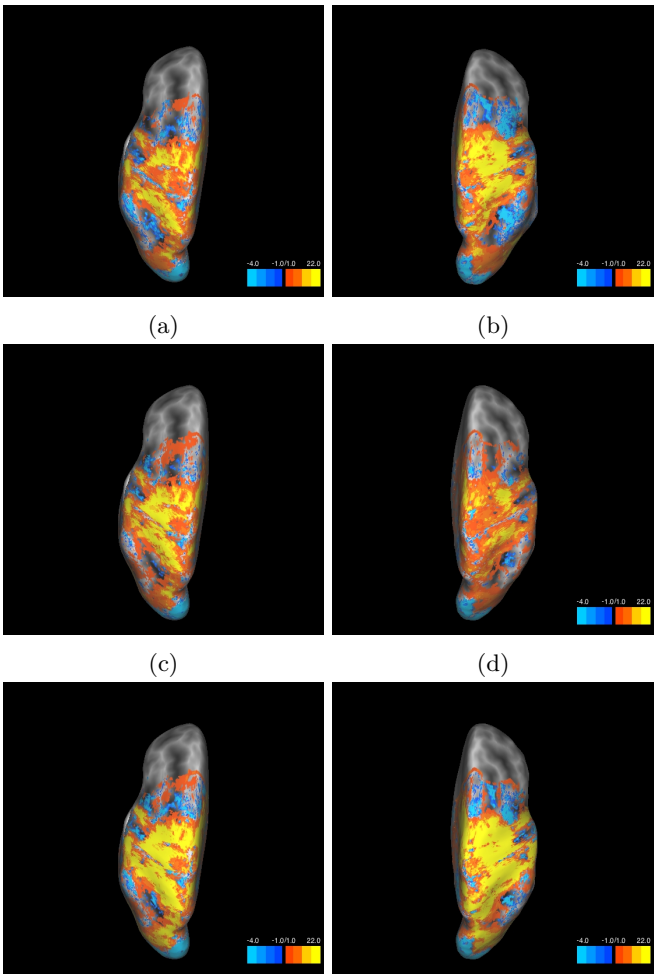

(a) (b) (c) (d) (e) (f)

Figure C.3: t-Contrast maps for unimanual left, unimanual right and bimanual movements for the Left and Right Hemispheres, Subj.No 3.

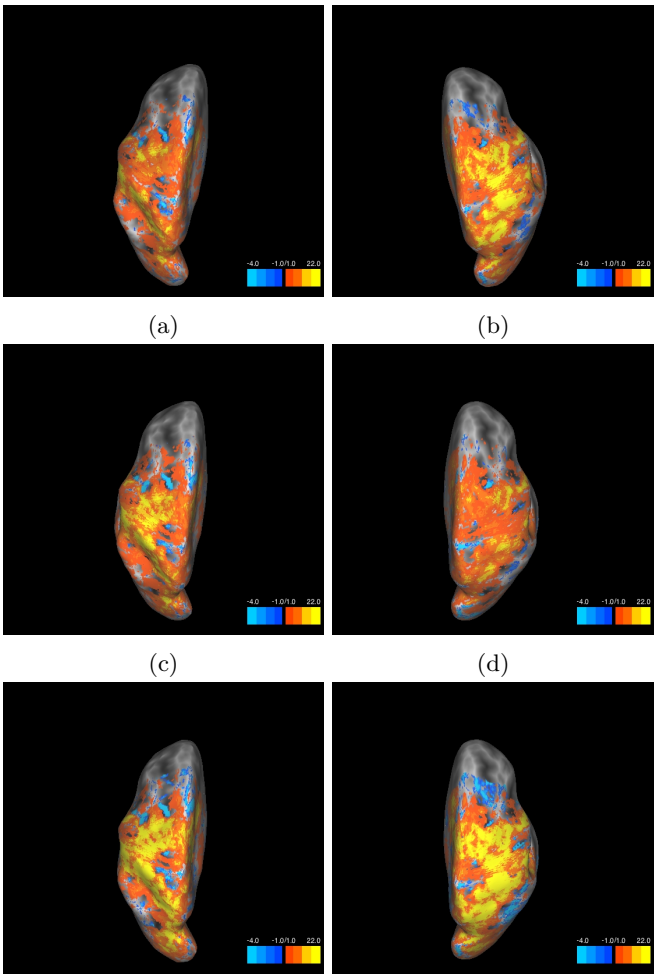

(a) (b)

(c) (d)

(e) (f)

Figure C.4: t-Contrast maps for unimanual left, unimanual right and bimanual movements for the Left and Right Hemispheres, Subj.No 4.

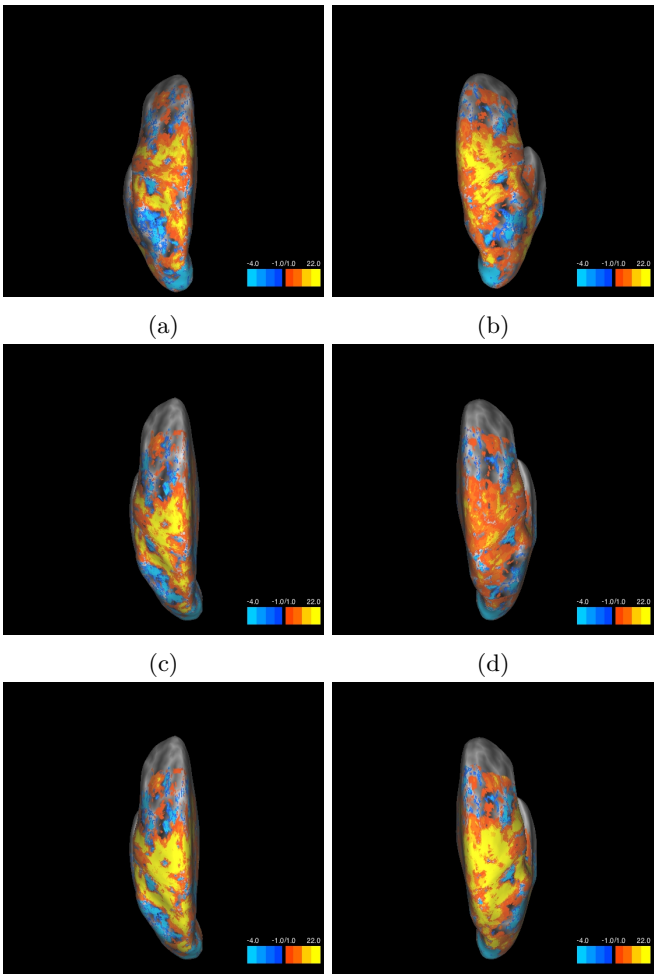

(a) (b)

(c) (d)

(e) (f)

Figure C.5: t-Contrast maps for unimanual left, unimanual right and bimanual movements for the Left and Right Hemispheres, Subj.No 5.

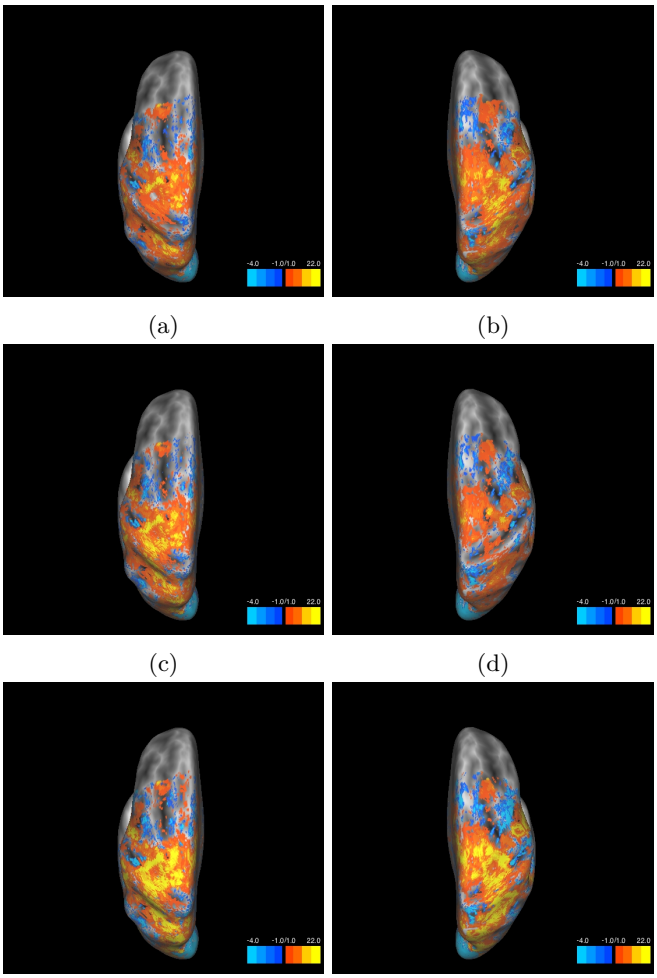

(a) (b)

(c) (d)

(e) (f)

Figure C.6: t-Contrast maps for unimanual left, unimanual right and bimanual movements for the Left and Right Hemispheres, Subj.No 6.

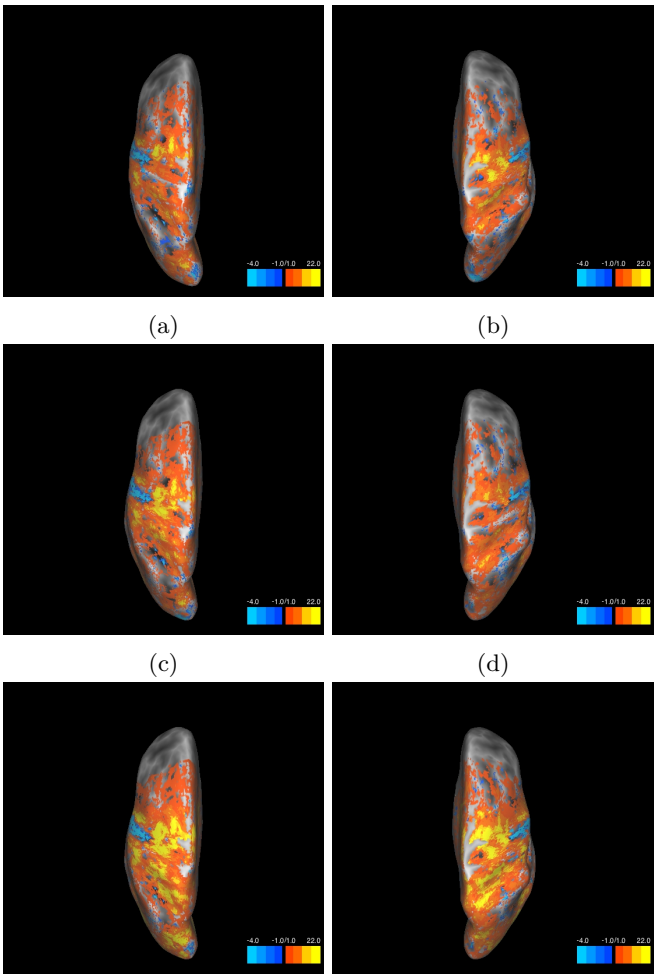

(a) (b) (c) (d) (e) (f)

Figure C.7: t-Contrast maps for unimanual left, unimanual right and bimanual movements for the Left and Right Hemispheres, Subj.No 7.

Appendix D

ROI Quantification of activity correlates

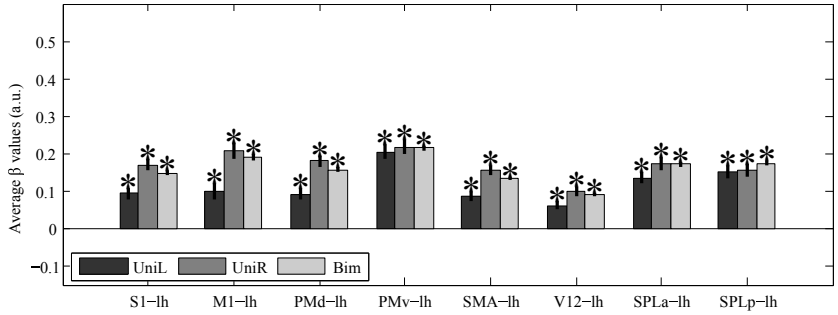

(a)

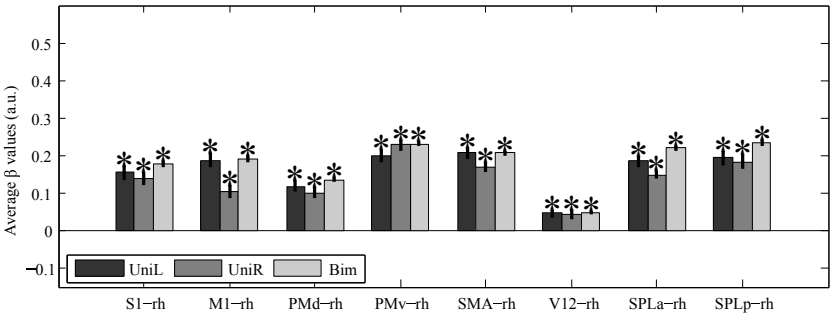

(b)

Figure D.1: Average beta-value across defined ROI's for S1. Error bars indicate standard error, and significance is marked by * - t-test under the null-hypothesis that the mean of the population is zero, $\alpha = 0.05$.

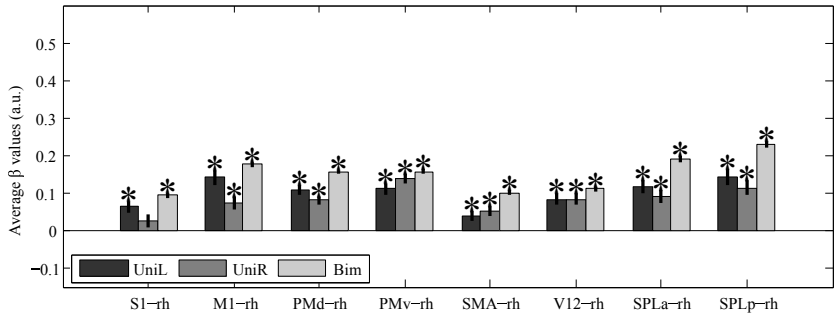

(a)

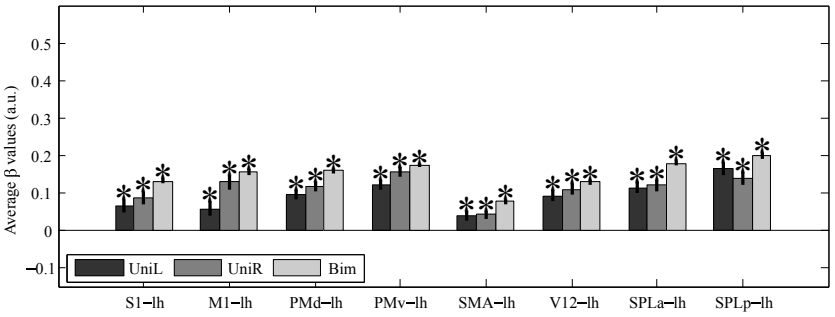

(b)

Figure D.2: Average beta-value across defined ROI's for S2. Error bars indicate standard error, and significance is marked by * - t-test under the null-hypothesis that the mean of the population is zero, $\alpha = 0.05$.

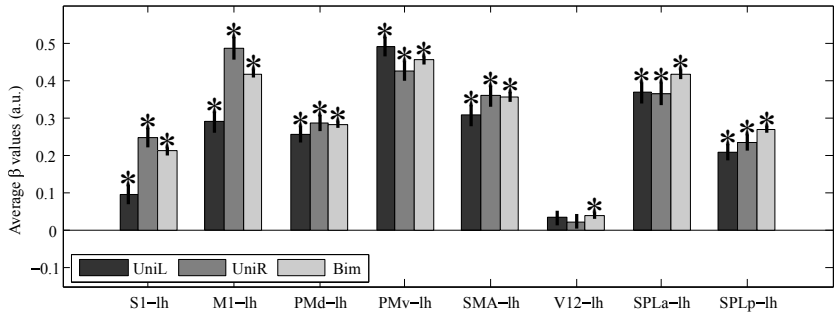

(a)

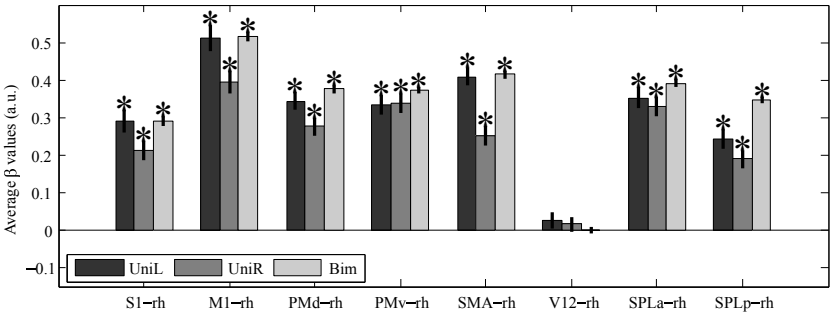

(b)

Figure D.3: Average beta-value across defined ROI's for S3. Error bars indicate standard error, and significance is marked by * - t-test under the null-hypothesis that the mean of the population is zero, $\alpha = 0.05$.

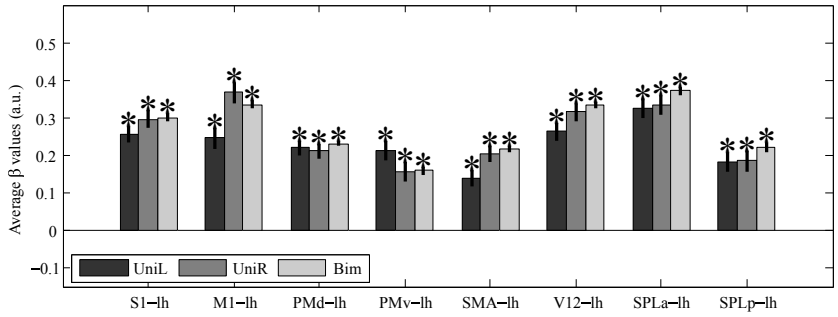

(a)

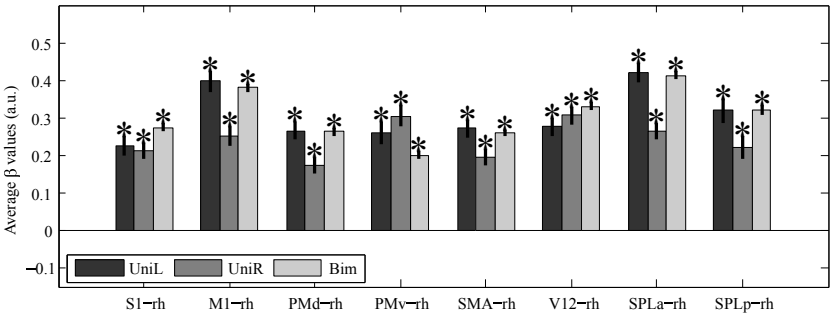

(b)

Figure D.4: Average beta-value across defined ROI's for S4. Error bars indicate standard error, and significance is marked by * - t-test under the null-hypothesis that the mean of the population is zero, $\alpha = 0.05$.

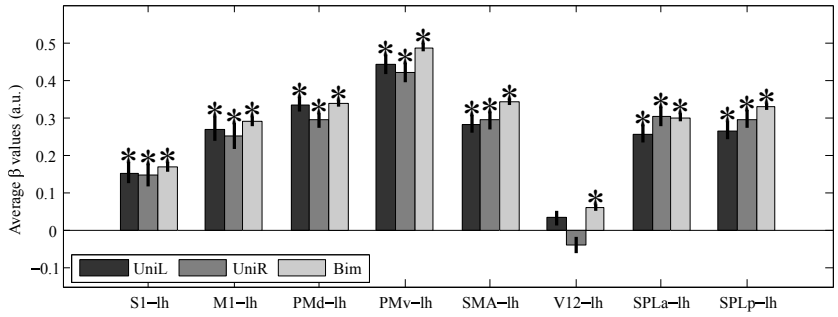

(a)

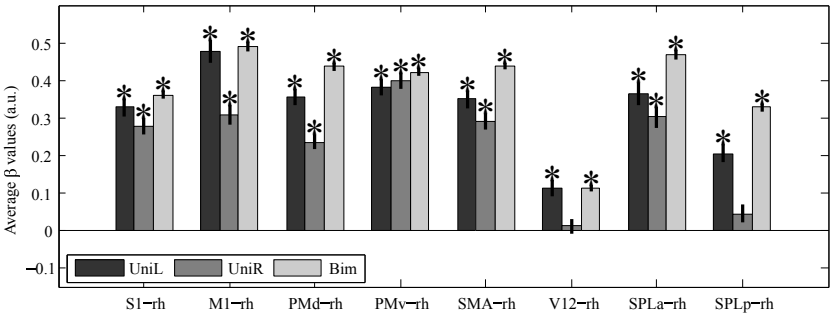

(b)

Figure D.5: Average beta-value across defined ROI's for S5. Error bars indicate standard error, and significance is marked by * - t-test under the null-hypothesis that the mean of the population is zero, $\alpha = 0.05$.

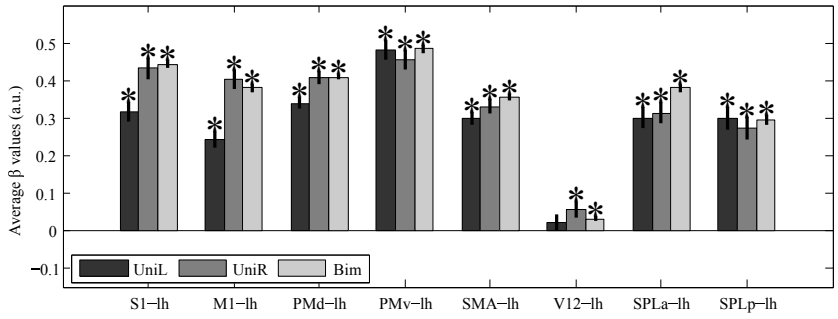

(a)

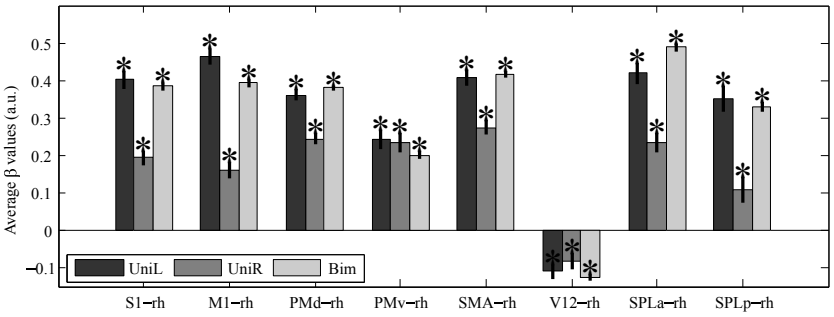

(b)

Figure D.6: Average beta-value across defined ROI's for S6. Error bars indicate standard error, and significance is marked by * - t-test under the null-hypothesis that the mean of the population is zero, $\alpha = 0.05$.

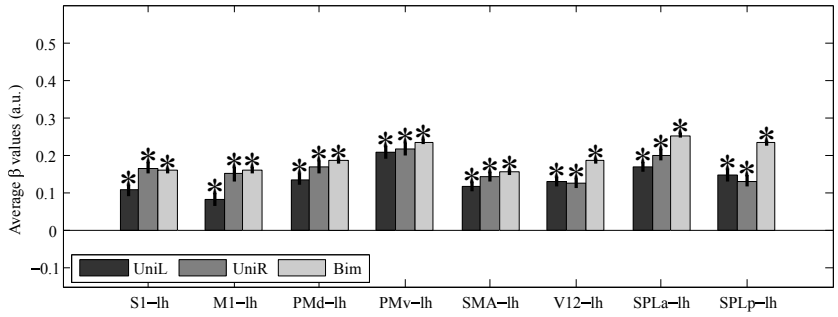

(a)

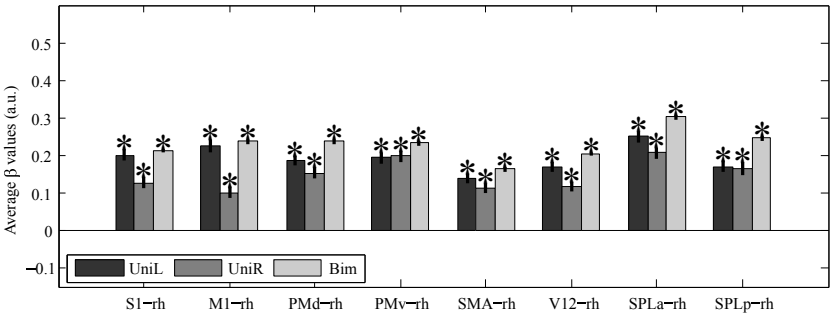

(b)

Figure D.7: Average beta-value across defined ROI's for S7. Error bars indicate standard error, and significance is marked by * - t-test under the null-hypothesis that the mean of the population is zero, $\alpha = 0.05$.

Appendix E

RDM sections

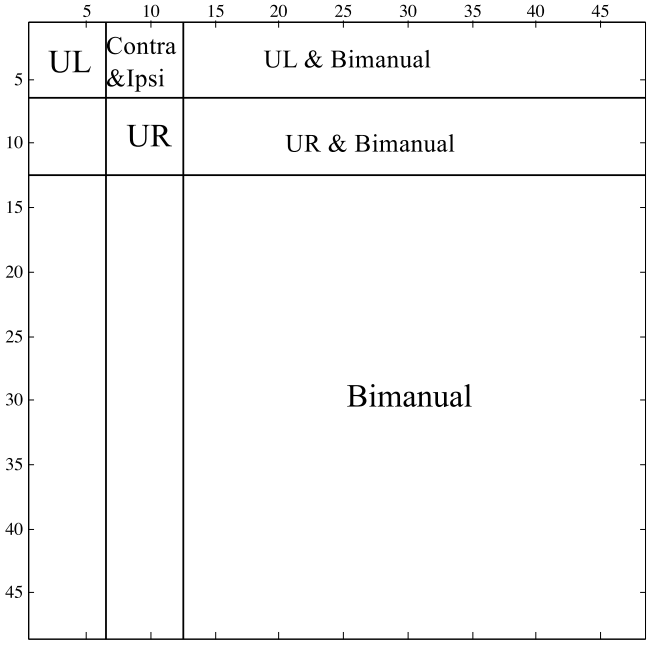

Figure E.1: Sections of representational dissimilarity matrices in this study. *UL* and *UR* indicate distances for unimanual left and right conditions, respectively. *Contra* & *Ipsi* refers to the distance between unimanual left and right patterns. The *Bimanual* part are the distances between bimanual conditions for all directional combinations. *UL* & *Bimanual* and *UR* & *Bimanual* contain the distances between each of the unimanual and bimanual movements.

Appendix F

RDMs

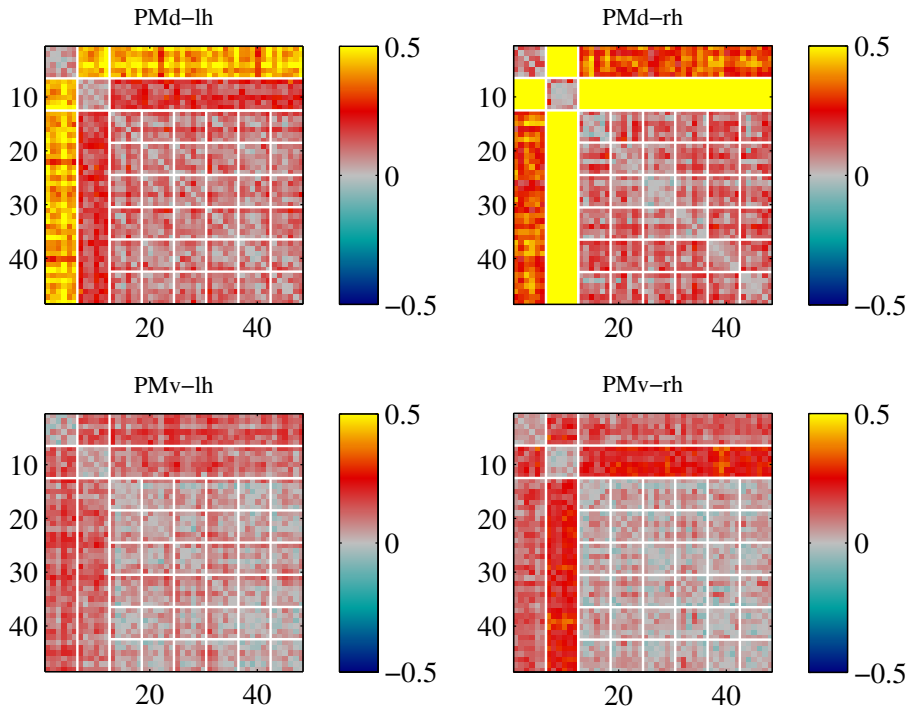

(a)

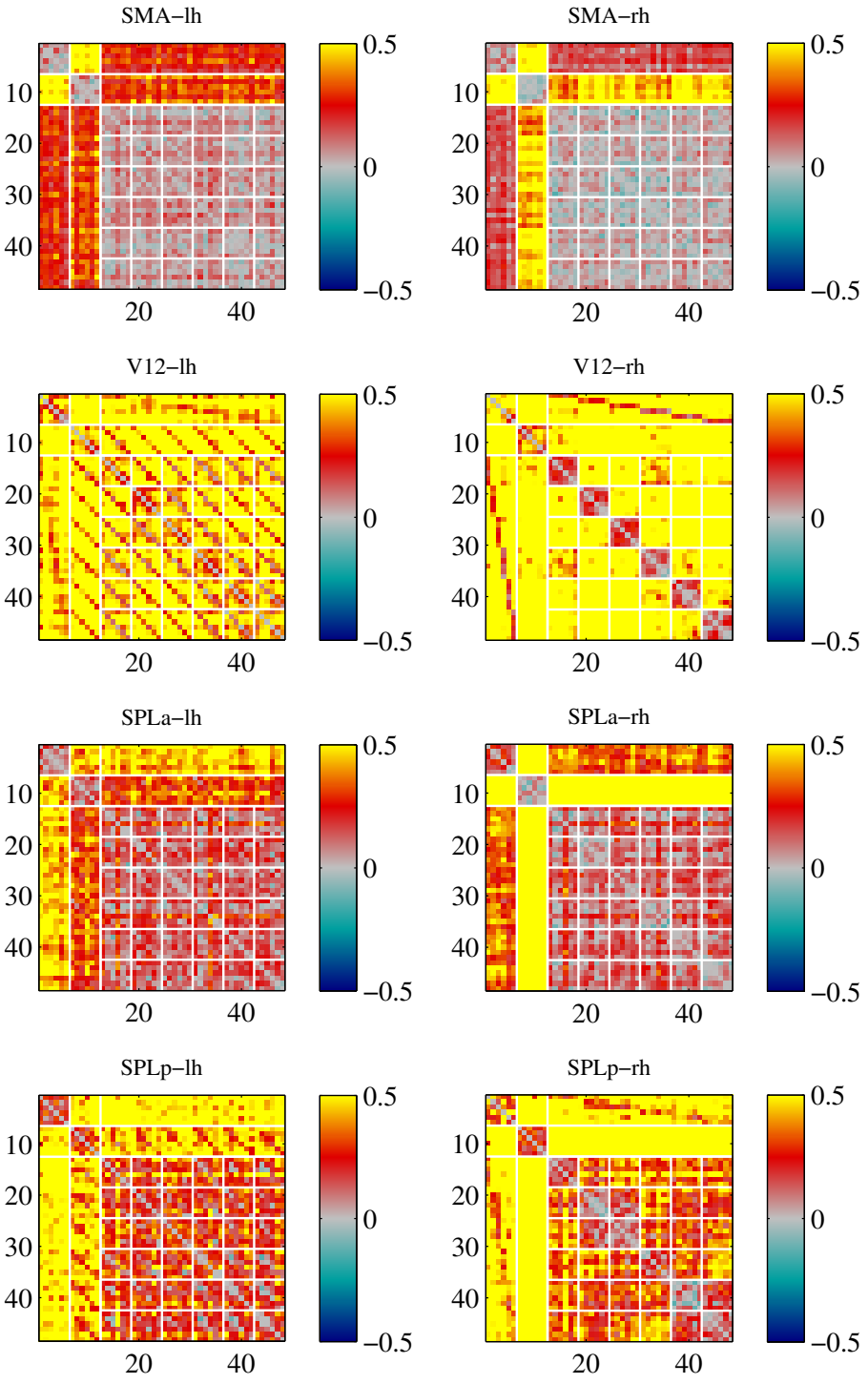

(b)

Figure F.1: RDMs averaged across all Full Study Subjects for the the remaining regions of interest in the left and right hemispheres. Each value in the RDMs is the squared distance in voxel space, between every two conditions (arbitrary units).

Appendix G

Inter-Subject RDM correlations

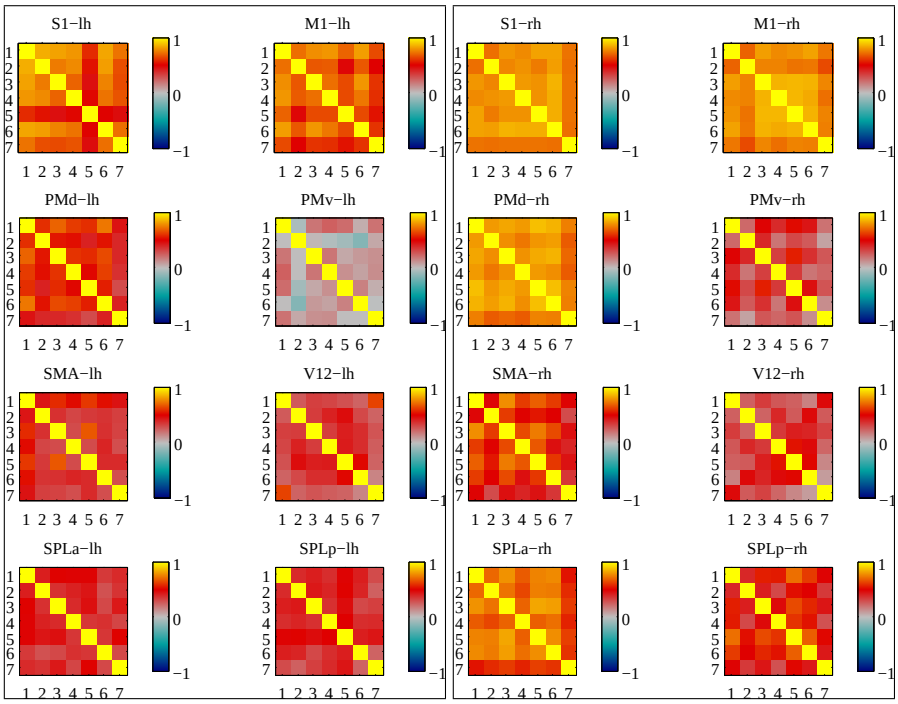

Figure G.1: Inter-subject correlations of RDMs at each ROI. Box on the left corresponds to the Left Hemisphere. Box on the right corresponds to the Right Hemisphere.

Appendix H

Bimanual Tuning Maps

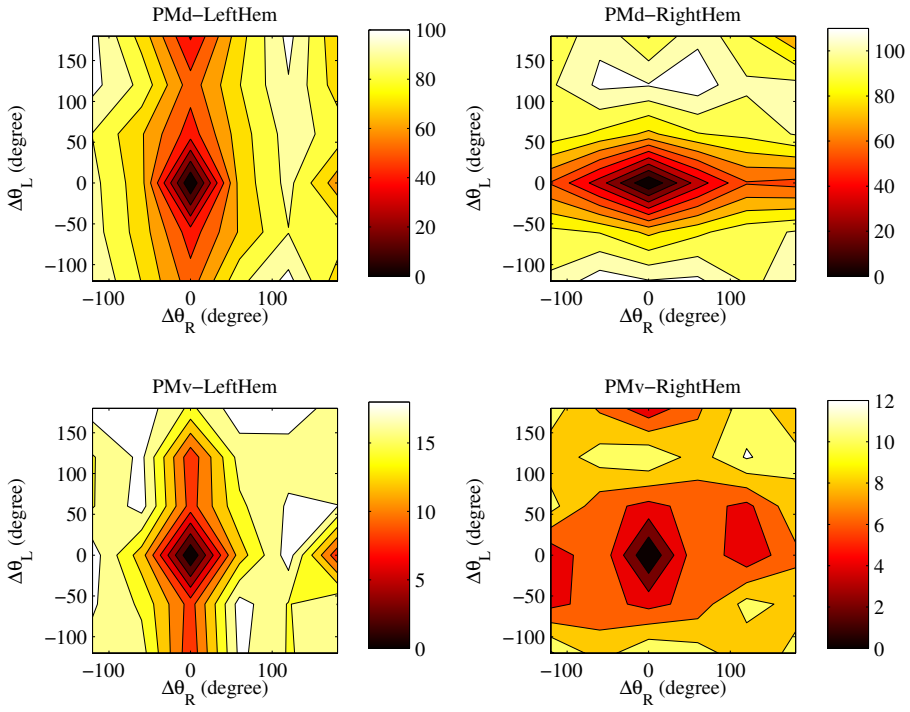

(a)

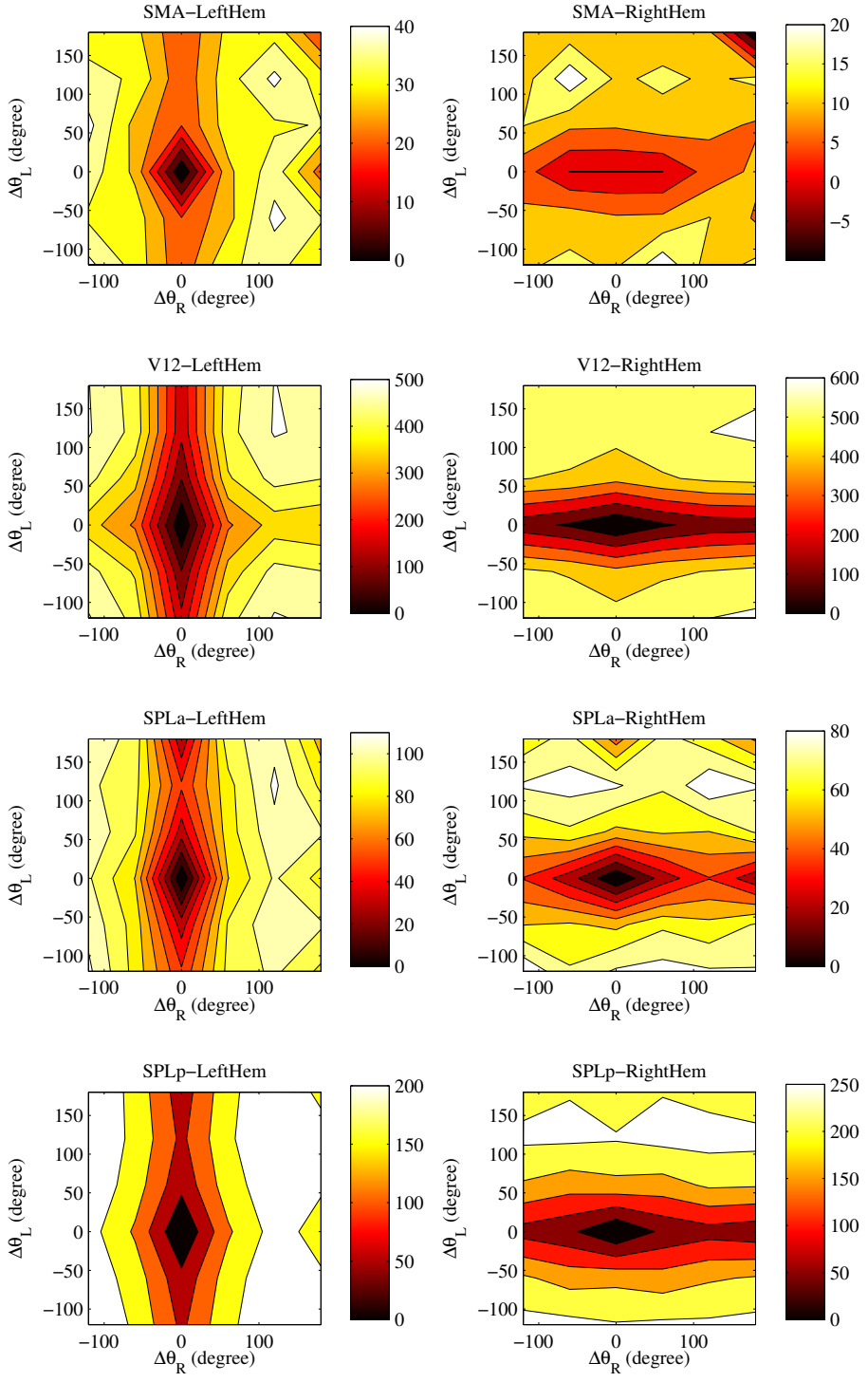

(b)

Figure H.1: Bimanual tuning maps for PMd, PMv (*a*) and SMA, V12, SPLa and SPLp (*b*) for the left and right hemispheres for the specified ROI's, obtained by re-organizing the RDMs and averaging squared distance values (arbitrary units, distance before normalization by number of voxels).

References

[1] Kandel ER, Schwartz JH, Jessel TM. Principles of Neural Science. 4th ed. New York: McGraw-Hill; 2000.

[2] Georgopoulos AP, Kalaska JF, Caminiti R, Massey JT. On the relations between the direction of two-dimensional arm movements and cell discharge in primate motor cortex. The Journal of neuroscience : the official journal of the Society for Neuroscience. 1982 Nov;2(11):1527–37.

[3] Donchin O, Gribova A, Steinberg O, Bergman H, Vaadia E. Primarymotor cortex is involved in bimanual coordination. Nature. 1998;395(6699):274–278.

[4] Ganguly K, Secundo L, Ranade G, Orsborn A, Chang EF, Dimitrov DF, et al. Cortical representation of ipsilateral arm movements in monkey and man. The Journal of neuroscience : the official journal of the Society for Neuroscience. 2009 Oct;(41):12948–56.

[5] Diedrichsen J, Wiestler T, Krakauer JW. Two distinct ipsilateral cortical representations for individuated finger movements. Cerebral cortex (New York, NY : 1991). 2013 Jun;23(6):1362–77.

[6] Rokni U, Steinberg O, Vaadia E, Sompolinsky H. Cortical representation of bimanual movements. The Journal of neuroscience : the official journal of the Society for Neuroscience. 2003;23(37):11577–11586.

[7] Yokoi A, Hirashima M, Nozaki D. Gain field encoding of the kinematics of both arms in the internal model enables flexible bimanual action. The Journal of neuroscience : the official journal of the Society for Neuroscience. 2011 Nov;31(47):17058–68.

[8] Allievi AG, Melendez-Calderon A, Arichi T, Edwards AD, Burdet E. An fMRI compatible wrist robotic interface to study brain development in neonates. Annals of biomedical engineering. 2013 Jun;41(6):1181–92.

[9] Brown GG, Perthen JE, Liu TT, Buxton RB. A primer on functional magnetic resonance imaging. Neuropsychology review. 2007 Jun;17(2):107–25.

[10] Classen J, Liepert J, Wise SP, Hallett M, Cohen LG. Rapid plasticity of human cortical movement representation induced by practice. Journal of neurophysiology. 1998;79(2):1117–1123.

[11] Liepert J, Graef S, Uhde I, Leidner O, Weiller C. Training-induced changes of motor cortex representations in stroke patients. Acta Neurologica Scandinavica. 2000 May;101(5):321–326.

[12] Ejaz N, Hamada M, Diedrichsen J. Hand use predicts the structure of representations in sensorimotor cortex. Nature Neuroscience. 2015;103(June).

[13] Martin JH. The corticospinal system: from development to motor control. The Neuroscientist : a review journal bringing neurobiology, neurology and psychiatry. 2005;11(2):161–173.

[14] Eisenberg M, Shmuelof L, Vaadia E, Zohary E. Functional organization of human motor cortex: directional selectivity for movement. The Journal of neuroscience : the official journal of the Society for Neuroscience. 2010 Jun;30(26):8897–905.

[15] Strick PL. Stimulating research on motor cortex. Nature neuroscience. 2002;5(8):714–715.

[16] Georgopoulos A. Higher order motor control. Annual Review of Neuroscience. 1991;14:361–377.

[17] Graziano MSA, Taylor CSR, Moore T. Complex movements evoked by microstimulation of precentral cortex. Neuron. 2002;34(5):841–851.

[18] Serge Chassagnon, Lorella Minotti, Stéphane Kremer, Dominique Hoffmann, Philippe Kahane. Somatosensory, motor, and reaching/grasping responses to direct electrical stimulation of the human cingulate motor areas. Journal of Neurosurgery. 2008;109(4):593–604.

[19] Shenoy KV, Sahani M, Churchland MM. Cortical control of arm movements: a dynamical systems perspective. Annual review of neuroscience. 2013;36:337–59.

[20] Georgopoulos A, Caminiti R. Spatial coding of movement: a hypothesis concerning the coding of movement direction by motor cortical populations. Exp Brain Research. 1983;7.

[21] Georgopoulos AP, Kettner RE, Schwartz AB. Primate motor cortex and free arm movements to visual targets in three-dimensional space. II. Coding of the direction of movement by a neuronal population. The Journal of neuroscience : the official journal of the Society for Neuroscience. 1988;8(8):2928–2937.

[22] Taira M, Boline J, Smyrnis N, Georgopoulos AP, Ashe J. On the relations between single cell activity in the motor cortex and the direction and magnitude of three-dimensional static isometric force. Experimental brain research Experimentelle Hirnforschung Experimentation cerebrale. 1996;109(3):367–376.

[23] Sergio LE, Hamel-Pâquet C, Kalaska JF. Motor cortex neural correlates of output kinematics and kinetics during isometric-force and arm-reaching tasks. Journal of neurophysiology. 2005;94(4):2353–2378.

[24] Mahan MY, Georgopoulos AP. Motor directional tuning across brain areas: directional resonance and the role of inhibition for directional accuracy. Frontiers in neural circuits. 2013;7(May):92.

[25] Gourtzelidis P, Tzagarakis C, Lewis SM, Crowe Da, Auerbach E, Jerde Ta, et al. Mental maze solving: Directional fMRI tuning and population coding in the superior parietal lobule. Experimental Brain Research. 2005;165(3):273–282.

[26] Amirikian B, Georgopulos aP. Directional tuning profiles of motor cortical cells. Neuroscience research. 2000 Jan;36(1):73–9.

[27] Howard IS, Franklin DW. Neural Tuning Functions Underlie Both Generalization and Interference. PLoS ONE. 2015;10(6):1–21.

[28] Kakei S, Hoffman DS, Strick PL. Muscle and Movement Representations in the Primary Motor Cortex. Science. 1999 Sep;285(5436):2136–2139.

[29] Swinnen SP, Wenderoth N. Two hands, one brain: Cognitive neuroscience of bimanual skill. Trends in Cognitive Sciences. 2004;8(1):18–25.

[30] Peper CLE, Beek PJ, van Wieringen PCW. Frequency-induced phase transitions in bimanual tapping. Biological Cybernetics. 1995;73(4):301–309.

[31] Lee TD, Swinnen SP, Verschueren S. Relative Phase Alterations during Bimanual Skill Acquisition. Journal of Motor Behavior. 1995 Sep;27(3):263–274.

[32] Li Y, Levin O, Forner-Cordero A, Ronsse R, Swinnen SP. Coordination of complex bimanual multijoint movements under increasing cycling frequencies: The prevalence of mirror-image and translational symmetry. Acta Psychologica. 2009;130(3):183–195.

[33] Spijkers W, Heuer H. Structural Constraints on the Performance of Symmetrical Bimanual Movements with Different Amplitudes. The Quarterly Journal of Experimental Psychology Section A. 1995;48(3):716–740.

[34] Franz Ea, Eliassen JC, Ivry RB, Gazzaniga MS. Dissociation of Spatial and Temporal Coupling in the Bimanual Movements of Callosotomy Patients. Psychological Science. 1996;7(5):306–310.

[35] Swinnen SP, Jardin K, Meulenbroek R, Dounskaia N, Den Brandt MHV. Egocentric and Allocentric Constraints in the Expression of Patterns of Interlimb Coordination. Journal of Cognitive Neuroscience. 1997;9(3):348–377.

[36] Swinnen SP, Jardin K, Verschueren S, Meulenbroek R, Franz L, Dounskaia N, et al. Exploring interlimb constraints during bimanual graphic performance: Effects of muscle grouping and direction. Behavioural Brain Research. 1998;90(1):79–87.

[37] Lee TD, Blandin Y, Proteau L. Effects of task instructions and oscillation frequency on bimanual coordination. Psychological research. 1996;59(2):100–106.

[38] Diedrichsen J, Hazeltine E, Kennerley S, Ivry RB. Moving to Directly Cued Locations Abolishes Spatial Interference During Bimanual Actions. Psychological Science. 2001 Nov;12(6):493–498.

[39] Brinkman C. Supplementary motor area of the monkey's cerebral cortex: short-and long-term deficits after unilateral ablation and the effects of subsequent callosal section. The Journal of neuroscience. 1984;4:918–929.

[40] Tanji J, Okano K, Sato K. Relation of neurons in the nonprimary motor cortex to bilateral hand movement. Nature. 1987;.

[41] Koeneke S, Lutz K, Wüstenberg T, Jäncke L. Bimanual versus unimanual coordination: what makes the difference? NeuroImage. 2004 Jul;22(3):1336–50.

[42] Walsh RR, Small SL, Chen EE, Solodkin a. Network activation during bimanual movements in humans. NeuroImage. 2008 Nov;43(3):540–53.

[43] Heitger MH, Macé MJM, Jastorff J, Swinnen SP, Orban GA. Cortical regions involved in the observation of bimanual actions. Journal of Neurophysiology. 2012 Nov;108(9):2594–2611.

[44] Franz EA, Waldie KE, Smith MJ. The Effect of Callosotomy on Novel Versus Familiar Bimanual Actions: A Neural Dissociation Between Controlled and Automatic Processes? Psychological Science. 2000 Jan;11(1):82–85.

[45] Swinnen SP. Intermanual coordination: from behavioural principles to neural-network interactions. Nature reviews Neuroscience. 2002 May;3(5):348–59.

[46] Debaere F, Wenderoth N, Sunaert S, Van Hecke P, Swinnen SP. Internal vs external generation of movements: Differential neural pathways involved in bimanual coordination performed in the presence or absence of augmented visual feedback. NeuroImage. 2003;19(3):764–776.

[47] Oliveira FTP, Ivry RB. The Representation of Action: Insights From Bimanual Coordination. Current Directions in Psychological Science. 2008 Apr;17(2):130–135.

[48] Diedrichsen J, Grafton S, Albert N, Hazeltine E, Ivry RB. Goal-selection and movement-related conflict during bimanual reaching movements. Cerebral Cortex. 2006;16(12):1729–1738.

[49] Johnson-Frey SH. The neural bases of complex tool use in humans. Trends in Cognitive Sciences. 2004;8(2):71–78.

[50] Donchin O. Primary and Supplementary Cortex in Bimanual Movements: A Study of Cortical Physiology. 1999;(December).

[51] Soteropoulos DS, Edgley SA, Baker SN. Lack of evidence for direct corticospinal contributions to control of the ipsilateral forelimb in monkey. The Journal of neuroscience : the official journal of the Society for Neuroscience. 2011 Aug;31(31):11208–19.

[52] Tazoe T, Perez MA. Speed-dependent contribution of callosal pathways to ipsilateral movements. The Journal of neuroscience : the official journal of the Society for Neuroscience. 2013 Oct;33(41):16178–88.

[53] Hummel FC, Cohen LG. Non-invasive brain stimulation: a new strategy to improve neurorehabilitation after stroke? Lancet Neurology. 2006;5(8):708–712.

[54] Lee M, Hinder MR, Gandevia SC, Carroll TJ. The ipsilateral motor cortex contributes to cross-limb transfer of performance gains after ballistic motor practice. The Journal of physiology. 2010 Jan;588(Pt 1):201–12.

[55] Bradnam LV, Stinear CM, Byblow WD. Ipsilateral motor pathways after stroke: implications for non-invasive brain stimulation. Frontiers in human neuroscience. 2013 Jan;7(May):184.

[56] Huettel SA, Song AW, McCarthy G. Functional Magnetic Resonance Imaging. 2nd ed. Sunderland: Sinauer Associates, Inc; 2008.

[57] Hillary FG, DeLuca J. Functional Neuroimaging in Clinical Populations. 1st ed. New York: The Guilford Press; 2007.

[58] McRobbie D, Moore E, Graves M, Prince M. MRI from Picture to Proton. 2nd ed. Cambridge University Press; 2006.

[59] Bernstein M, King K, Zhou X. Handbook of MRI pulse sequences. 1st ed. San Diego: Academic Press Inc.; 2004.

[60] Friston KJ, Penny WD, Ashburner J, Kiebel SJ, Nichols TE. Statistical parametric mapping : the analysis of functional brain images. Academic Press; 2007.

[61] Friston KJ, Holmes aP, Worsley KJ, Poline JP, Frith CD, Frackowiak RSJ. Statistical parametric maps in functional imaging: A general linear approach. Human Brain Mapping. 1995;2(4):189–210.

[62] Norman KA, Polyn SM, Detre GJ, Haxby JV. Beyond mind-reading: multi-voxel pattern analysis of fMRI data. Trends Cogn Sci. 2006;10(9):424–430.

[63] Haxby JV, Connolly AC, Guntupalli JS. Decoding Neural Representational Spaces Using Multivariate Pattern Analysis. Annual review of neuroscience. 2014 Jun;37:435–456.

[64] Pereira F, Mitchell T, Botvinick M. Machine learning classifiers and fMRI: A tutorial overview. NeuroImage. 2009;45:S199–S209.

[65] Kriegeskorte N, Mur M, Bandettini P. Representational similarity analysis - connecting the branches of systems neuroscience. Frontiers in systems neuroscience. 2008 Jan;2(November):4.

[66] Nili H, Wingfield C, Walther A, Su L, Marslen-Wilson W, Kriegeskorte N. A Toolbox for Representational Similarity Analysis. PLoS Computational Biology. 2014;10(4).

[67] Patton J, Dawe G, Scharver C, Mussa-Ivaldi F, Kenyon R. Robotics and virtual reality: a perfect marriage for motor control research and rehabilitation. Assistive technology : the official journal of RESNA. 2006;18(2):181–195.

[68] Acosta AM, Kirsch RF, Perreault EJ. A robotic manipulator for the characterization of two-dimensional dynamic stiffness using stochastic displace-

ment perturbations. Journal of Neuroscience Methods. 2000;102(2):177–186.

[69] Franklin DW, Burdet E, Osu R, Kawato M, Milner TE. Functional significance of stiffness in adaptation of multijoint arm movements to stable and unstable dynamics. Experimental Brain Research. 2003;151(2):145–157.

[70] Ariff G, Donchin O, Nanayakkara T, Shadmehr R. A real-time state predictor in motor control: study of saccadic eye movements during unseen reaching movements. The Journal of neuroscience : the official journal of the Society for Neuroscience. 2002;22(17):7721–7729.

[71] Ernst MO, Banks MS. Humans integrate visual and haptic information in a statistically optimal fashion. Nature. 2002;415(6870):429–433.

[72] Gassert R, Burdet E, Chinzei K. Opportunities and challenges in MR-compatible robotics. Engineering in Medicine and Biology. 2008;(June):15–22.

[73] Gassert R, Burdet E, Chinzei K. MRI-compatible robotics. Engineering in Medicine and .... 2008;(June):25–27.

[74] Arichi T, Moraux A, Melendez A, Doria V, Groppo M, Merchant N, et al. Somatosensory cortical activation identified by functional MRI in preterm and term infants. NeuroImage. 2010 Feb;49(3):2063–71.

[75] Wiestler T, Waters-Metenier S, Diedrichsen J. Effector-independent motor sequence representations exist in extrinsic and intrinsic reference frames. The Journal of neuroscience : the official journal of the Society for Neuroscience. 2014 Apr;34(14):5054–64.

[76] fMRI robot;. Available from: `http://www.fmrirobot.org/`.

[77] Esmaeili M, Dailey W, Burdet E, Campolo D. Ergonomic design of a wrist exoskeleton and its effects on natural motor strategies during redundant tasks. 2013 IEEE International Conference on Robotics and Automation. 2013 May;p. 3370–3375.

[78] Home — SketchUp; 2014. Available from: `http://www.sketchup.com/`.

[79] Bourns Rotary Position Sensors - Datasheet;. Available from: `http://www.mouser.com/ds/2/54/3382-553069.pdf`.

[80] Sensoray s626 - Space Saving Multifunction Analog/Digital I/O;. Available from: `http://www.sensoray.com/products/626.htm`.

[81] Celozzi S, Feliziani M. EMP-coupling to twisted-wire cables. IEEE International Symposium on Electromagnetic Compatibility. 1990;.

[82] RSA Toolbox — Cognition and Brain Sciences Unit;. Available from: `http://www.mrc-cbu.cam.ac.uk/methods-and-resources/toolboxes/license/`.

[83] SPM8 - Statistical Parametric Mapping;. Available from: `http://www.fil.ion.ucl.ac.uk/spm/software/spm8/`.

[84] FreeSurfer;. Available from: `http://surfer.nmr.mgh.harvard.edu/`.

[85] Caret - Van Essen Lab;. Available from: http://brainvis.wustl.edu/wiki/index.php/Caret:About.

[86] Critchley F. On Certain Linear Mappings Between Inner-Product and Squared-Distance Matrices. Elsevier Inc. 1988;107(1988):91–107.

[87] Walther A, Ejaz N, Kriegeskorte N, Diedrichsen J. Representational fMRI analysis : an introductory tutorial; 2016.

[88] Yokoi A, Hirashima M, Nozaki D. Lateralized sensitivity of motor memories to the kinematics of the opposite arm reveals functional specialization during bimanual actions. The Journal of neuroscience : the official journal of the Society for Neuroscience. 2014 Jul;34(27):9141–51.

[89] Wiestler T, Diedrichsen J. Skill learning strengthens cortical representations of motor sequences. eLife. 2013;2013(2):1–20.

[90] Meyer DE, Smith JE, Wright CE. Models for the speed and accuracy of aimed movements. Psychological review. 1982 sep;89(5):449–482.